

1 **Impacts of an aerosol layer on a mid-latitude continental system of cumulus clouds:**  
2 **how do these impacts depend on the vertical location of the aerosol layer?**

3

4 Seoung Soo Lee<sup>1,2</sup>, Junshik Um<sup>3,4</sup>, Won Jun Choi<sup>5</sup>, Kyung-Ja Ha<sup>2,4,6</sup>, Chang Hoon Jung<sup>7</sup>,  
5 Jianping Guo<sup>8</sup>, Youtong Zheng<sup>9</sup>

6

7 <sup>1</sup>Earth System Science Interdisciplinary Center, University of Maryland, Maryland, USA

8 <sup>2</sup>Research Center for Climate Sciences, Pusan National University, Busan, Republic of

9 Korea

10 <sup>3</sup>Department of Atmospheric Sciences, Pusan National University, Busan, Republic of

11 Korea

12 <sup>4</sup>BK21 School of Earth and Environmental Systems, Pusan National University, Busan,

13 Republic of Korea

14 <sup>5</sup>National Institute of Environmental Research, Incheon, Republic of Korea

15 <sup>6</sup>Center for Climate Physics, Institute for Basic Science, Busan, Republic of Korea

16 <sup>7</sup>Department of Health Management, Kyungin Women's University, Incheon, Republic of

17 Korea

18 <sup>8</sup>State Key Laboratory of Severe Weather, Chinese Academy of Meteorological Sciences,

19 Beijing, China

20 <sup>9</sup>The Program in Atmospheric and Oceanic Sciences, Princeton University, Princeton,

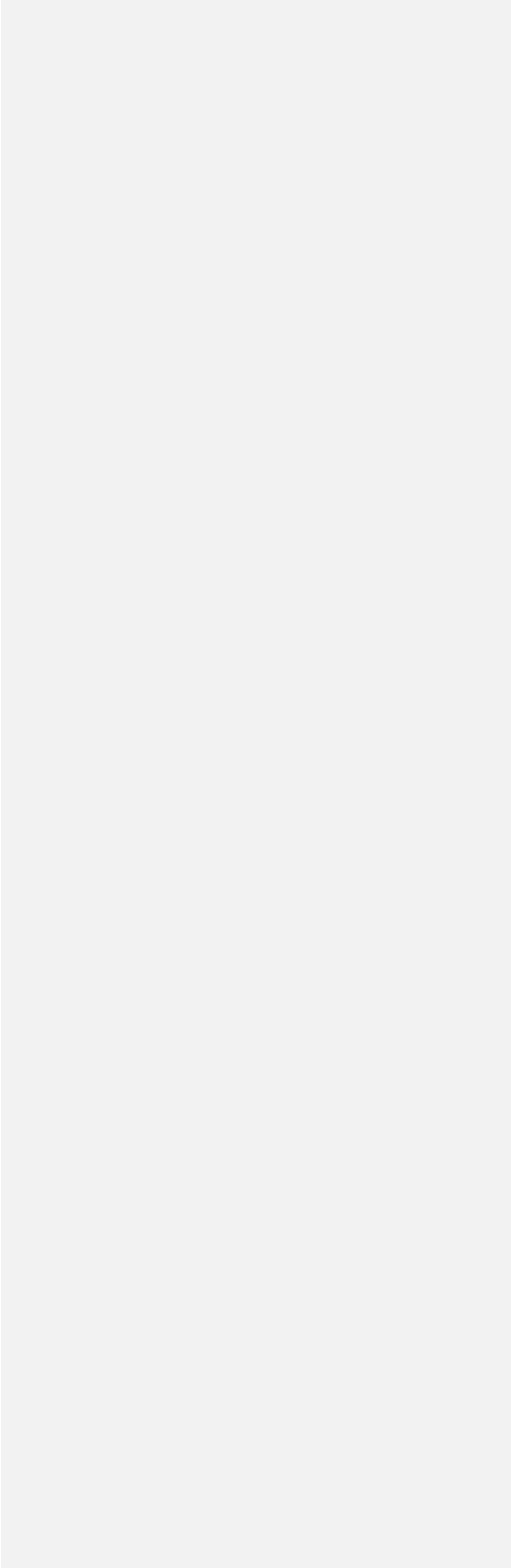
21 New Jersey, USA

22

23

24

25 Corresponding authors: Seoung Soo Lee and Junshik Um  
26 E-mail: [cumulss@gmail.com](mailto:cumulss@gmail.com), [slee1247@umd.edu](mailto:slee1247@umd.edu), [jjunum@pusan.ac.kr](mailto:jjunum@pusan.ac.kr)  
27  
28  
29  
30  
31  
32  
33  
34  
35  
36  
37  
38  
39  
40  
41  
42  
43  
44  
45  
46  
47  
48  
49  
50  
51



52 **Abstract**

53

54 ~~E~~ffects of an aerosol layer on warm cumulus clouds in the Korean Peninsula when the layer  
 55 is above ~~or~~ around the cloud tops ~~in the upper atmosphere~~ are compared to those effects  
 56 when ~~the layer~~ is around ~~or~~ below the cloud bases ~~in the low atmosphere~~. For this  
 57 comparison, simulations are performed using the large-eddy simulation framework. ~~When~~  
 58 the aerosol layer is in the low atmosphere, aerosols absorb solar radiation and radiatively  
 59 heat up air enough to induce greater instability, stronger updrafts and more cloud mass than  
 60 when the layer is in the upper atmosphere. Hence, there is the variation of cloud mass with  
 61 the location (or altitude) of the aerosol layer. It is found that this variation of cloud mass  
 62 reduces, as aerosol concentrations in the layer decrease or aerosol impacts on radiation are  
 63 absent. ~~The transportation of aerosols by updrafts reduces aerosol concentrations in the low~~  
 64 ~~atmosphere. This in turn reduces the aerosol radiative heating, updraft intensity and cloud~~  
 65 ~~mass.~~

66

67

68

69

70

71

72

73

74

75

76

77

78

79

80

81

82

**Deleted:** Using the large-eddy simulation framework,**Deleted:** e**Deleted:** or**Deleted:** in the upper atmosphere**Deleted:** examined. Also, these effects are compared to**Deleted:** of an aerosol layer**Deleted:** it**Deleted:** or**Deleted:** in the low atmosphere**Deleted:** Simulations show that**Deleted:** w**Deleted:** As aerosol concentrations in the layer decrease,

**Deleted:** the aerosol radiative heating gets weaker to lead to less instability, weaker updrafts and less cloud mass when the layer is in the low atmosphere. This in turn makes differences in cloud mass, which are between a situation when the layer is in the low atmosphere and that when the layer is in the upper atmosphere, smaller. It is found that the transportation of aerosols by updrafts reduces aerosol concentrations in the aerosol layer, which is in the low atmosphere, and in turn reduces the aerosol radiative heating, updraft intensity and cloud mass. It is also found that the presence of aerosol impacts on radiation suppresses updrafts and reduces clouds. Aerosols affect not only radiation but also aerosol activation. In the absence of aerosol impacts on radiation, aerosol impacts on the droplet nucleation increases cloud mass when the layer is in the low atmosphere as compared to a situation when the layer is in the upper atmosphere. As aerosol impacts on radiation team up with those on the droplet nucleation, differences in cloud mass, which are between a situation when the layer in the low atmosphere and that when the layer is in the upper atmosphere, get larger. This is as compared to a situation when there is no aerosol impacts on radiation and only aerosol impacts on the droplet nucleation.

## 1. Introduction

Warm cumulus clouds play an important role in global hydrologic and energy circulations (Warren et al., 1986; Stephens and Greenwald, 1991; Hartmann et al., 1992; Hahn and Warren, 2007; Wood, 2012). ~~Aerosols act as radiation absorbers, and they absorb solar radiation and heat up the atmosphere to change atmospheric stability. This in turn affects thermodynamics in cumulus clouds (Hansen et al., 1997). When these aerosols act as cloud condensation nuclei (CCN), they have an impact on aerosol activation and subsequent microphysical processes in cumulus clouds (Albrecht, 1989). However, these aerosol effects on warm cumulus clouds are highly uncertain and thus cause the highest uncertainty in the prediction of future climate (Ramaswamy et al., 2001; Forster et al., 2007).~~

In recent years, people have started to take interest in how aerosol layers affect clouds when these layers are above or around the tops of clouds (e.g., de Graaf et al., 2014; Xu et al., 2017). This interest is motivated by aerosol layers that are originated from biomass burning sites in the southern Africa (Mari et al., 2008; Menut et al., 2018; Haslett et al., 2019; Denjean et al., 2020). These layers are lifted and transported to the southeast Atlantic (SEA) region and located above or around the top of a large layer or deck of warm cumulus and stratocumulus clouds (Roberts et al., 2009; van der Werf et al., 2010; Che et al., 2022). Note that aerosols in the transported aerosol layers contain organic and black carbon, and these aerosols act as radiation absorbers as well as CCN (Wilcox, 2010; Deaconu et al., 2019; Chaboureau et al., 2022). Reflecting the interest, to better understand roles of aerosol layers above or around cloud tops in cloud development, there were international field campaigns in the SEA such as the National Aeronautics and Space Administration Observations of Aerosols above CLouds and their intEractionS (ORACLES; <https://espo.nasa.gov/oracles/content/ORACLES>), the United Kingdom Clouds and Aerosol Radiative Impacts and Forcing (CLARIFY; Redemann et al., 2021) and the French Aerosol, Radiation and Clouds in southern Africa (AEROCLO-sA; Formenti et al., 2019) campaigns.

Despite above-mentioned field campaigns, effects of aerosols above or around cloud tops have not been examined as much as those of aerosols around or below cloud bottoms (Haywood and Shine, 1997; Johnson et al., 2004; McFarquhar and Wang, 2006). Motivated

### Moved (insertion) [3]

~~Deleted:~~ When these

~~Deleted:~~ a

~~Deleted:~~ ,

~~Deleted:~~ the

~~Deleted:~~ , the

~~Deleted:~~ hydrologic and energy circulations, and climate

~~Deleted:~~ ,

~~Deleted:~~ and precipitation

~~Deleted:~~ the

~~Deleted:~~ , those circulations and climate

~~Deleted:~~ With industrialization, there have been significant increases in concentrations of aerosols acting as cloud condensation nuclei (CCN) and these increases are known to decrease droplet size (Twomey, 1974, 1977). Increases in concentrations of aerosols acting as radiation absorbers are also known to enhance the radiative heating of air by aerosols. These aerosol-induced changes in droplet size and radiative heating affect updrafts, cloud mass, cloud albedo and precipitation (Albrecht, 1989; Hansen et al., 1997). Global hydrologic and energy circulations are eventually affected by these aerosol effects.

~~Deleted:~~ , which are particularly

~~Deleted:~~ ,

~~Deleted:~~ act to

~~Deleted:~~

~~Deleted:~~ effects of

~~Deleted:~~ s

~~Deleted:~~ on clouds

~~Deleted:~~

~~Deleted:~~ that play an important role in global hydrologic and energy circulations

~~Deleted:~~ carbon (OC) and

~~Deleted:~~ (BC)

~~Deleted:~~ that

~~Deleted:~~ cloud condensation nuclei (

~~Deleted:~~ )

**Moved up [3]:** When these aerosols act as radiation absorbers, they absorb solar radiation and heat up the atmosphere to change atmospheric stability. This in turn affects the cumulus clouds, the hydrologic and energy circulations, and climate. When these aerosols act as CCN, they have an impact on aerosol activation,

~~Deleted:~~ and an associated potential importance of aerosol layer [1]

~~Deleted:~~ and its impacts on climate

~~Deleted:~~ NASA

~~Deleted:~~ It is well-known that the relative vertical location of [2]

~~Deleted:~~ d

~~Deleted:~~ previous studies on

~~Deleted:~~ aerosol-cloud interactions have focused mainly on effects [3]

~~Deleted:~~ on clouds

by this, this study delves into effects of not only aerosols around or below cloud bottoms but also those above or around cloud tops. Through this, this study aims to contribute to the more comprehensive understanding of aerosol-radiation-cloud interactions. This more comprehensive understanding in turn contributes to more general parameterizations of those interactions for climate and weather-forecast models. To fulfill the aim, this study adopts the large-eddy simulation (LES) framework and an idealized setup for the aerosol layer.

## 2. Case, model and simulations

### 2.1 LES model

The Advanced Research Weather Research and Forecasting (ARW) model is used for LES simulations in this study. The ARW model is a compressible model with a nonhydrostatic status. A 5th-order monotonic advection scheme is used to advect microphysical variables (Wang et al., 2009). The ARW adopts a bin scheme, which is detailed in Khain et al. (2011), to parameterize microphysics. A set of kinetic equations is solved by the bin scheme to represent size distribution functions for each class of hydrometeors and aerosols acting as cloud condensation nuclei (CCN). The hydrometeor classes are water drops, ice crystals (plate, columnar and branch types), snow aggregates, graupel and hail. There are 33 bins for each size distribution in a way that the mass of a particle  $m_j$  in the  $j$  bin is to be  $m_j = 2m_{j-1}$ .

Aerosol sinks and sources, which include aerosol advection and activation, control the evolution of aerosol size distribution at each grid point. For example, activated particles are emptied in the corresponding bins of the aerosol spectra. Aerosol mass included in hydrometeors, after activation, is moved to different classes and sizes of hydrometeors through collision-coalescence and removed from the atmosphere once hydrometeors that contain aerosols reach the surface.

The Rapid Radiation Transfer Model (RRTM; Mlawer et al., 1997) has been coupled to the bin microphysics scheme. Aerosols before their activation can affect radiation by changing the reflection, scattering, and absorption of radiation. This radiative effect of

**Deleted:** Effects of aerosols above or around cloud tops on clouds have not been examined as much.

**Deleted:** Hence,

**Moved (insertion) [1]**

**Deleted:** enhance our

**Deleted:** effects of the relative location of an aerosol layer and a cloud deck on the cloud deck

**Deleted:** This contributes to the low-level understanding of effects of the relative location of an aerosol layer and a cloud deck on the cloud deck. Improving this understanding, which is about going beyond the traditional approach that focuses on around- or below-cloud-bottom aerosol layers, is likely to contribute to the more comprehensive understanding of aerosol-cloud-radiation interactions and

**Deleted:** thus

**Deleted:** those interactions

**Moved up [1]:** Hence, this study aims to enhance our understanding of effects of the relative location of an aerosol layer and a cloud deck on the cloud deck.

**Deleted:** This aim is pursued by investigating aerosol-cloud-radiation interactions in a typical situation where an aerosol layer is around or below the bottom of a system of warm cumulus clouds. Then, to fulfill the aim, these interactions in the typical situation are compared to a situation where an aerosol layer is around or above the top of the system.

**Deleted:** In this study,

**Deleted:** the investigation is performed by using simulations

**Deleted:** ing

**Deleted:** .

**Deleted:** which is based on observation,

**Deleted:** The Hebrew University Cloud Model (HUCM) detailed in Khain et al. (2011) is the bin scheme.

**Deleted:** These sinks and sources include advection and aerosol activation (Fan et al., 2009).

**Deleted:** A

**Deleted:** described above

278 aerosol is represented following Feingold et al. (2005). The internal aerosol mixture and  
 279 the ARW relative humidity are used to calculate the hygroscopic growth of the aerosol  
 280 particles as well as their optical properties. In practice, optical property calculations with  
 281 the consideration of the hygroscopic growth are performed offline prior to simulation and  
 282 stored in lookup tables. Calculations are done for the prescribed aerosol size distribution  
 283 and composition, and unit concentration. During model runtime, grid-point number  
 284 concentration and relative humidity determine the look-up table entries that specify the  
 285 grid-point aerosol optical properties and are fed into the RRTM to simulate the radiative  
 286 effect of aerosol. The effective sizes of hydrometeors are calculated in the bin scheme and  
 287 the calculated sizes are transferred to the RRTM to consider effects of the effective sizes  
 288 on radiation.

289 The presence of aerosol perturbs the radiative fluxes reaching the surface, and its  
 290 subsequent partitioning into sensible and latent heat fluxes (i.e., the Bowen ratio). This is  
 291 accounted for with the interactive Noah land surface model (Chen and Dudhia, 2001).

## 293 2.2 Case and simulations

### 295 2.2.1 Case and standard simulations

297 There is an observed system of warm cumulus clouds in a domain in the Korean Peninsula  
 298 on April 13<sup>th</sup>, 2016. The domain is marked in Figure 1a. Figure 2 shows the field of the  
 299 cloud reflectivity observed by the Communication, Ocean, and Meteorological Satellite  
 300 (COMS). This field is at 14:00 LST on April 13<sup>th</sup>, 2016 when the system is around the  
 301 mature stage in the domain. The ratio of the reflected radiative flux by an object to the  
 302 incident radiative flux on it is the reflectivity (Liou, 2002) and thus unitless. In Figure 2,  
 303 we see cloud cells that are elongated in the southwest-northeast direction due to the  
 304 southwesterly wind.

305 The cloud system is simulated for a period between 10:00 and 18:00 LST on April 13<sup>th</sup>,  
 306 2016. This period includes a time span over which the system exists. For the simulation  
 307 (i.e., the control run), a 50-m resolution is used for the horizontal domain. The length of  
 308 the domain in both the east-west and north-south directions is 20 km. In the vertical domain,

**Deleted:** , represented by extinction, single scattering albedo, and asymmetry factor. Aerosol uptake of water vapor is considered over the range of relative humidity in the domain.

**Deleted:** hygroscopic growth and

**Deleted:** an

**Deleted:** adopted microphysics scheme

**Deleted:** the

**Deleted:**

**Deleted:** , as

**Deleted:** l

**Formatted:** Superscript

**Formatted:** Superscript

**Formatted:** Font: (Asian) Batang

**Formatted:** Font: (Asian) Batang

**Deleted:** ,

**Deleted:** :00

**Deleted:** :00

**Deleted:** 2015

**Deleted:** . This system is simulated to fulfill the goal of this study.

**Deleted:** a three-dimensional

**Deleted:** of the system in the domain over the period

**Deleted:** (north-south)

**Deleted:** (20)

328 the resolution coarsens with height. The resolution in the vertical domain is 20 m just above  
 329 the surface and 100 m at the model top ~~that is at ~4.5 km in altitude. The time step or~~  
 330 ~~temporal resolution is set at 0.1 second.~~ Initial and boundary conditions of potential  
 331 temperature, specific humidity, and wind for the simulation are provided by reanalysis data.  
 332 These data ~~represent the synoptic-scale environment and~~ are produced by the Met Office  
 333 Unified Model (Brown et al., 2012) every 6 hours on a  $0.11^\circ \times 0.11^\circ$  grid. ~~Figure 3 depicts~~  
 334 the vertical distributions of potential temperature and water-vapor mixing ratio at 09:00  
 335 LST on April 13<sup>th</sup>, 2016 in radiosonde sounding that is obtained near the domain as marked  
 336 in Figure 1a. This vertical distribution represents initial environmental conditions for the  
 337 control run. The conditional instability is present in the vertical profiles and this favors the  
 338 development of warm cumulus clouds. An open lateral boundary condition is employed  
 339 for the run.

340 ~~Not only~~ a site of the aerosol robotic network (AERONET; Holben et al., 2001) ~~but~~  
 341 ~~also ground stations that measure PM<sub>2.5</sub> are in the domain as marked in Figure 1b. The mass~~  
 342 ~~of aerosols with diameter smaller than 2.5  $\mu\text{m}$  per unit volume of the air is PM<sub>2.5</sub>. Around~~  
 343 ~~07:00 LST on April 13<sup>th</sup>, 2016, an aerosol layer advected from East Asia starts to be present~~  
 344 ~~in the domain. This advection of aerosols is monitored and identified by PM<sub>2.5</sub> which is~~  
 345 ~~measured by stations in the Yellow sea and domain (Eun et al., 2016; Ha et al., 2019; Lee~~  
 346 ~~et al., 2021). The station in the Yellow sea is marked in Figure 1a. Figure 4 shows the~~  
 347 ~~evolution of PM<sub>2.5</sub> at the station in the Yellow sea and the average PM<sub>2.5</sub> over stations in~~  
 348 ~~the domain from 03:00 LST to 18:00 LST on April 13<sup>th</sup>, 2016. Due to the aerosol-layer~~  
 349 ~~advection from East Asia, aerosol mass starts to increase around 04:00 LST and reaches its~~  
 350 ~~peak around 08:00 LST at the station in the sea. Then, in the domain, aerosol mass starts~~  
 351 ~~to increase around 07:00 LST, and the mass attains its peak around 11:00 LST. This depicts~~  
 352 ~~a situation where aerosols or an aerosol layer advected from East Asia first arrives at the~~  
 353 ~~station in the Yellow sea around 04:00 LST and then further advected to the east to reach~~  
 354 ~~the domain and to start the increase in aerosol mass there around 07:00 LST.~~

355 According to the AERONET measurement at 12:00 LST, which is ~1 hour before  
 356 the observed cumulus clouds start to form, aerosol particles in the ~~advected aerosol~~ layer,  
 357 on average, are an internal mixture of 70 % ammonium sulfate, 22 % organic compound  
 358 and 8% black carbon. Aerosol chemical composition in this study is assumed to be

Deleted: that is

Deleted:

Deleted:

Deleted:

Deleted: These data represent the synoptic-scale environment.

Deleted: 2

Deleted: 5

Deleted: 2015

Deleted: .

Deleted: for the development of the clouds in

Deleted: e control run

Formatted: Font: (Asian) SimSun, (Asian) Chinese (China)

Deleted: Ther

Deleted: e

Deleted: is

Formatted: Subscript

Deleted:

Formatted: Font: (Asian) SimSun, (Asian) Chinese (China)

Deleted:

Deleted: At 10:00 LST when clouds in the domain start to develop

Deleted: , there is

Deleted: the

Deleted: and this layer causes aerosol pollution in the domain

Formatted: Font: (Asian) SimSun, (Asian) Chinese (China)

Deleted:

Formatted: Font: (Asian) SimSun, (Asian) Chinese (China), Subscript

Formatted: Font: (Asian) SimSun, (Asian) Chinese (China)

Deleted: aerosol-

Deleted: ing

Deleted: as described in Lee et al. (2021)

Formatted: Font: (Asian) SimSun, (Asian) Chinese (China)

Formatted: Superscript

Formatted: Automatically adjust right indent when grid is defined, Adjust space between Latin and Asian text, Adjust space between Asian text and numbers

Deleted:

Formatted: Font: (Asian) SimSun, (Asian) Chinese (China)

Formatted: Font: (Asian) SimSun, (Asian) Chinese (China)

Formatted: Font: (Asian) SimSun, (Asian) Chinese (China)

384 represented by this mixture in the whole domain during the whole simulation period. Based  
 385 on the AERONET observation, the shape of the initial size distribution of aerosols acting  
 386 as CCN is assumed to follow a bi-modal log-normal distribution as shown in Figure 5 in  
 387 all parts of the domain. Modal radius of this distribution is 0.11 and 1.20  $\mu\text{m}$  and standard  
 388 deviation of this distribution is 1.71 and 1.92, while the partition of aerosol number, which  
 389 is normalized by the total aerosol number of the size distribution, is 0.999 and 0.001 for  
 390 accumulation and coarse modes, respectively. The total aerosol number concentration in  
 391 the advected aerosol layer based on the AERONET-observed size distribution is  $\sim 15000$   
 392  $\text{cm}^{-3}$ . This concentration is applied to all grid points in the aerosol layer at the first time  
 393 step of the control run. This aerosol layer is idealized to be located around or below cloud  
 394 bases between the surface and 1.0 km. Cloud bases are located around 1.0 km. At 06:00  
 395 LST,  $\sim 1$  hour before the advected aerosol layer starts to be present, the AERONET-  
 396 measured aerosol concentration is  $\sim 150 \text{ cm}^{-3}$  in the domain. This aerosol concentration is  
 397 assumed to be a background aerosol concentration that is not affected by the advected  
 398 aerosol layer. Based on this assumption, the initial aerosol concentration is set at  $150 \text{ cm}^{-3}$   
 399 outside the layer.

400 This study compares aerosol effects on warm cumulus clouds when the aerosol layer  
 401 is above or around the cloud tops to those effects when the layer is around or below the  
 402 cloud bases. For this, we repeat the control run by moving the aerosol layer upward to  
 403 altitudes between 2.5 and 3.5 km. Here, initial aerosol concentrations in and outside the  
 404 aerosol layer are  $15000 \text{ cm}^{-3}$  and  $150 \text{ cm}^{-3}$ , respectively, in both of the runs. Altitudes  
 405 between 2.5 and 3.5 km are places where cloud tops are located frequently and the  
 406 simulated maximum cloud-top height is 3.3 km. This repeated run is referred to as the aro-  
 407 above-cld run.

408 It is well-known that aerosol-cloud-radiation interactions are strongly dependent on  
 409 aerosol concentrations (Tao et al., 2012). Hence, we want to test how results in the control  
 410 and aro-above-cld runs are sensitive to aerosol concentrations in the aerosol layer. For the  
 411 test, the control and aro-above-cld runs are repeated with 10 times lower initial aerosol  
 412 concentrations in the aerosol layer but with no changes in initial aerosol concentrations  
 413 outside the layer. In these repeated runs, the aerosol concentration in the aerosol layer at

Deleted: s

Deleted: background

Formatted: Font: (Asian) SimSun, (Asian) Chinese (China)

Formatted: Font: (Asian) SimSun, (Asian) Chinese (China)

Deleted: It is assumed that the size distribution of background aerosols acting as CCN in all parts of the domain during the whole simulation period is assumed to follow the bi-modal size distribution. The average aerosol concentration in the layer over the domain at 10:00 LST is

Deleted: average

Formatted: Font: (Asian) SimSun, (Asian) Chinese (China)

Deleted:

Deleted: and

Deleted: as shown in Figure 3a

Formatted: Font: (Asian) SimSun, (Asian) Chinese (China)

Formatted: Font: (Asian) SimSun, (Asian) Chinese (China)

Formatted: Font: (Asian) SimSun, (Asian) Chinese (China)

Formatted: Font: (Asian) SimSun, (Asian) Chinese (China)

Formatted: Font: (Asian) SimSun, (Asian) Chinese (China)

Formatted: Font: (Asian) SimSun, (Asian) Chinese (China), Superscript

Formatted: Font: (Asian) SimSun, (Asian) Chinese (China)

Formatted: Font: (Default) Times New Roman, (Asian) SimSun, 12 pt, Font color: Auto, (Asian) Chinese (China)

Formatted: Font: (Default) Times New Roman, (Asian) SimSun, 12 pt, Font color: Auto, (Asian) Chinese (China)

Formatted: Superscript

Formatted: Font: (Default) Times New Roman, (Asian) SimSun, 12 pt, Font color: Auto, (Asian) Chinese (China)

Deleted: Above the layer, aerosol concentration is assumed to be  $150 \text{ cm}^{-3}$ .

Deleted: aims to

Deleted: understand differences in

Deleted: between the situation where an aerosol layer is above and around the cloud tops and that where the aerosol layer is around and below the cloud bases.

Deleted: To fulfill this goal

Deleted: an idealized setup where

Deleted: r is moved

Deleted: as shown in Figure 3b

Deleted: . Note that

Deleted: As shown in Figures 3a and 3b, aerosol concentrations are

Deleted: W

Deleted: main

Deleted: main

Deleted: in the domain

Deleted: e main aerosol

Deleted: main



the first time step is  $1500 \text{ cm}^{-3}$ . Henceforth, the repeated control and aro-above-cld runs are referred to as the control-1500 and aro-above-cld-1500 runs.

## 2.2.2 Additional simulations

Clouds affect aerosols through cloud processes such as nucleation of droplets and aerosol transportation (or advection) by cloud-induced wind. Updrafts and downdrafts comprise cloud-induced wind and transport aerosols upward and downward, respectively. Motivated by this, we take interest in impacts of clouds on aerosols and how these impacts in turn change the influence of aerosols on clouds. To examine this aspect of aerosol-cloud interactions, the above-mentioned four standard simulations (i.e., the control, aro-above-cld, control-1500 and aro-above-cld-1500 runs) are repeated. In these repeated runs, aerosol concentrations at each grid point, which are set at the first time step, do not vary with time or are not affected by cloud processes. These repeated runs are referred to as the control-novary, aro-above-cld-novary, control-1500-novary, and aro-above-cld-1500-novary runs. By comparing the standard simulations to these repeated ones, we aim to identify how cloud processes affect the aerosol layer and then the impacts of the layer on clouds.

In this study, we also aim to better understand roles of the interception (e.g., reflection, scattering and absorption) of radiation by aerosols in impacts of the aerosol layer on clouds. This interception of radiation by aerosols, which is referred to as aerosol radiative effects, results in phenomena such as radiative heating of air by aerosols. To better understand roles of aerosol radiative effects, the above four standard simulations are repeated again by turning off aerosol radiative effects. These repeated runs are the control-norad, aro-above-cld-norad, control-1500-norad, aro-above-cld-1500-norad runs. The summary of simulations in this study is given in Table 1.

## 3. Results

### 3.1 The control and aro-above-cld runs

Deleted:

Deleted: by

Deleted: Here

Deleted: are interested

Deleted: affect

Deleted: aerosol effects

Deleted: amine these

Deleted: s

Deleted: e

Deleted: g

Deleted: by preventing aerosol evolution with time at each grid point. In other words,

Deleted: i

Deleted: s

Deleted: such as nucleation and advection

Deleted: roles of cloud impacts on aerosols in aerosol-layer impacts on clouds are identified.

Deleted: , which

Deleted: These roles are referred to as aerosol radiative effects.

Deleted:

501 Figure 6 shows the time- and area-averaged vertical distributions of cloud-liquid mass  
 502 density for the standard simulations. In Figure 6, the cloud layer is between 1.0 and 3.3 km  
 503 in the control run and between 0.8 and 2.6 km in the aro-above-cld run. The time- and  
 504 domain-averaged cloud-liquid mass density is  $0.7$  and  $1.3 \times 10^{-3} \text{ g m}^{-3}$  in the control run  
 505 and in the aro-above-cld run, respectively. Hence, we see that clouds are thicker with their  
 506 higher tops and have greater mass in the control run than in the aro-above-cld run.

507 We utilize satellite and ground observations to evaluate the control run. The Moderate  
 508 Resolution Imaging Spectroradiometer (MODIS) is a representative sensor on board polar-  
 509 orbiting satellites. The MODIS passes the domain only at 10:30 am and 1:30 pm on each  
 510 day. This means that it is difficult to get reliable data, which cover the whole simulation  
 511 period, from the MODIS. The COMS, which is a geostationary satellite and available in  
 512 East Asia, does not provide reliable data of cloud mass. However, comparatively reliable  
 513 data of cloud fraction and cloud-top height throughout the whole simulation period are  
 514 obtained from the COMS. Data of cloud fraction and cloud-bottom height over the whole  
 515 simulation period are collected from ground observations in the domain; note that ground  
 516 stations which measure PM<sub>2.5</sub> as marked in Figure 1b also measure cloud fraction and  
 517 cloud-bottom height. Here, cloud fraction and cloud-bottom height in the control run are  
 518 compared to those from ground observations. A comparison of cloud-top height is made in  
 519 the domain between the control run and the COMS. Cloud fraction, which is averaged over  
 520 all time points with non-zero cloud fraction over the whole simulation period, is 0.25 in  
 521 the control run. Cloud fraction is 0.21 when it is averaged over all time points with non-  
 522 zero cloud fraction that are collected from all ground stations in the domain over the whole  
 523 simulation period. Cloud-bottom height, which is averaged over all air columns with non-  
 524 zero cloud-bottom height over the whole simulation period, is 1.1 km in the control run.  
 525 Cloud-bottom height is 1.0 km, when it is averaged over all time points with non-zero  
 526 cloud-bottom height that are collected from all ground stations in the domain over the  
 527 whole simulation period. The average cloud-top height over all air columns with non-zero  
 528 cloud-top height over the whole simulation period is 2.8 and 2.6 km in the control run and  
 529 observation, respectively. The difference in each of cloud fraction, cloud-bottom and -top  
 530 heights between the control run and observations is ~10%. This means that the control run  
 531 is performed reasonably well.

Deleted: 4

Deleted: that represents cloud mass

Deleted: 4

Deleted: This is despite the fact that aerosol concentrations in the main aerosol layer in the control run are identical to those in the aro-above-cld run. ...

538 Figure 7a shows the time series of the domain-averaged liquid-water path, which is  
 539 the vertical integral of cloud-liquid mass density, for the standard simulations. During the  
 540 initial stage of the cloud development between 12:50 and 13:50 LST, the average cloud  
 541 mass is slightly higher in the control run than in the aro-above-cld run. Also, the average  
 542 non-zero cloud mass starts to appear earlier in the control run. Over the period between  
 543 13:50 and 14:10 LST, there is a jump (or rapid increase or surge) in the average cloud mass  
 544 in the control run but not in the aro-above-cld run. During this period with the jump, at  
 545 some specific time points, the average mass is ~one order of magnitude higher in the  
 546 control run. Of interest is that just after the jump and at 14:10 LST, the average mass in the  
 547 control run starts to decrease and at 14:40 LST, becomes lower than that in the aro-above-  
 548 cld run. Hence, the greater time- and domain-averaged cloud mass in the control run is  
 549 mainly attributed to the jump. Figures 7b and 7c show the time series of the domain-  
 550 averaged updraft speed and condensation rates, respectively. These figures indicate that the  
 551 average updraft mass fluxes and associated condensation rates in the control run are also  
 552 slightly higher than in the aro-above-cld run for the period between 12:50 and 13:50 LST.  
 553 The average updraft speed and associated condensation rates jump and thus are much  
 554 higher in the control run during the period between ~13:50 and ~14:10 LST (Figures 7b  
 555 and 7c). After the jump, the speed and rates decrease rapidly and become lower in the  
 556 control run (Figures 7b and 7c). Condensation is the only source of cloud mass in warm  
 557 cumulus clouds. Also, updrafts with higher speeds tend to produce higher condensation  
 558 rates for a given environmental condition. Hence, cloud mass, condensation rate and the  
 559 updraft speed are closely linked to each other. This enables cloud mass, condensation rate  
 560 and the updraft speed to be similar in terms of their temporal evolution in each of the  
 561 control and aro-above-cld runs (Figures 7a, 7b and 7c).

562 Figure 7d shows the time series of the domain-averaged convective available potential  
 563 energy (CAPE) for the control and aro-above-cld runs. Considering that updrafts grow by  
 564 consuming buoyancy energy, updraft intensity is proportional to CAPE that is the integral  
 565 of the buoyancy energy in the vertical domain. Hence, the evolution of CAPE is similar to  
 566 that of the updraft speed, associated condensation rates and cloud mass (Figure 7). This  
 567 involves the jump not only in CAPE but also in those speed, rates and mass in the control  
 568 run.

Deleted: ¶  
 Deleted: 5  
 Deleted: and thus, represents cloud mass

Deleted: than in the aro-above-cld run

Deleted: than in the aro-above-cld run

Deleted: in cloud mass

Deleted: As seen in

Deleted: 5

Deleted: 5

Deleted: that

Deleted: ,

Deleted: in the control run

Deleted: in the control run

Deleted: , hence, these speed and rates are much higher in the control run than in the aro-above-cld run during the period between ~13:50 and ~14:10 LST

Deleted: 5

Deleted: 5

Deleted: than in the aro-above-cld run

Deleted: 5

Deleted: 5

Deleted: Taking into account the fact that

Deleted: c

Deleted: and the updraft speed strongly control the amount of condensation, the updraft speed, condensation rate and cloud mass in each of the runs and differences in those variables between the runs are similar in terms of their temporal evolution.¶

Deleted: 5

Deleted: in each of the runs

Deleted: Accordingly, the evolution of differences in CAPE between the runs is similar to that of those differences in the updraft speed, associated condensation rates and cloud mass.

Deleted: similarity includes

Deleted: during the period between 13:50 and 14:10 LST

Deleted: (052022)

604 In Figure 7, the peaks (or the maximum values) of the domain-averaged CAPE, the  
 605 updraft speed, condensation rates and cloud mass in the control run occur around 14:10  
 606 LST and this occurrence is earlier than that which occurs around 14:50 LST in the aro-  
 607 above-cld run. This means that the cloud system in the control run reaches its mature stage  
 608 earlier. Immediately after the peak around 14:10 LST, the system enters its dissipating  
 609 stage in the control run. However, the system enters its dissipating stage after 14:50 LST  
 610 in the aro-above-cld run. Hence, the cloud system in the control run matures and demises  
 611 faster. Stated differently, the cloud system in the control run has a shorter life cycle.

612 To find mechanisms controlling the jump in CAPE which is a main cause of the greater  
 613 cloud mass in the control run, the analysis of the results is done for an initial period between  
 614 10:00 LST and 13:50 LST which is immediately before the jump starts to occur. The  
 615 average net shortwave fluxes at the surface are shown in Table 2 for the initial period in  
 616 the control and aro-above-cld runs. Table 2 shows that during the initial period, there is a  
 617 smaller amount of the surface-reaching shortwave radiation in the control run than in the  
 618 aro-above-cld run. The aerosol layer intercepts solar radiation and reduces the surface-  
 619 reaching solar radiation. In spite of the fact that the initial depth of the aerosol layer and  
 620 aerosol concentrations in the layer are identical between the runs, results here indicate that  
 621 the aerosol layer in the low atmosphere is more efficient in the interception of solar  
 622 radiation than that in the upper atmosphere. Due to the less solar radiation reaching the  
 623 surface, the time- and area-averaged net surface heat fluxes, which are the sum of the  
 624 surface sensible and latent-heat fluxes, become lower in the control run during the initial  
 625 period (Table 2). Hence, the surface fluxes favor more instability or higher CAPE and  
 626 associated subsequent more intense updrafts and more cloud mass in the aro-above-cld run.

627 The vertical distributions of the time- and domain-averaged radiative heating rates are  
 628 obtained for the initial period. For the initial period, the average radiative heating rate is  
 629 much higher in the control run than in the aro-above-cld run particularly at altitudes  
 630 between 0.0 and ~1.0 km where cloud bases are located (Figure 8a). This is associated with  
 631 the fact that the aerosol layer is located at altitudes between 0.0 and 1.0 km in the control  
 632 run. This more radiative heating in the low atmosphere during the initial period results in  
 633 the subsequent jump in CAPE, associated higher CAPE, more intense updrafts and more  
 634 cloud mass after the initial period by outweighing the lower surface heat fluxes in the

Deleted: s

Deleted: 5

Deleted: s

Deleted: than that in the aro-above-cld run

Deleted: A

Deleted: ,

Deleted: while around 14:10 LST in the aro-above-cld run,

Deleted: still evolves to enter the mature stage and it

Deleted:

Deleted: as compared to that in the aro-above-cld run

Deleted: than that in the aro-above-cld run

Deleted: acts a

Deleted: when the simulation starts

Deleted: The thermodynamic condition for the CAPE jump is established during this initial period.

Deleted: in the control run

Deleted: that are incident on the surface

Deleted: which reaches the surface

Deleted: main

Deleted: than in the aro-above-cld run

Deleted: subsequent

Deleted: than in the control run

Deleted: for each of the control and aro-above-cld runs

Deleted:

Deleted: 6

Deleted: main

Deleted: favors

Deleted: , which involves its jump in the control run, in the control run than in the aro-above-cld run after the initial pe

control run. The aerosol layer is located at altitudes between 2.5 and 3.5 km, hence, the average radiative heating rate is higher around those altitudes in the aro-above-cld run (Figures 8a and 8b). However, this higher radiative heating rate is in the upper part of the domain and tends to induce more stabilization of the atmosphere in the aro-above-cld run. Thus, the higher radiative heating rate in the aro-above-cld run contributes to lower CAPE, less intense updrafts and less cloud mass in the aro-above-cld run especially for the period when the jumps occur in the control run.

### 3.2 Comparisons between simulations with different aerosol concentrations

With the lower concentration of aerosols in the aerosol layer, there are the much more surface-reaching solar radiation and resultant higher surface fluxes in the control-1500 run than in the control run and in the aro-above-cld-1500 run than in the aro-above-cld run (Table 2). This induces higher CAPE, stronger updrafts and more condensation and cloud mass in the control-1500 run than in the control run over most of the simulation period except for the period with the jump in CAPE in the control run, and in the aro-above-cld-1500 run than in the aro-above-cld run throughout the simulation period (Figure 7). This leads to the greater time- and domain-averaged cloud mass in the control-1500 run than in the control run and in the aro-above-cld-1500 run than in the aro-above-cld run (Figure 6). Regarding the control and control-1500 runs, this is despite the fact that aerosol radiative heating in the low atmosphere is higher due to higher aerosol concentrations there in the control run than in the control-1500 run (Figure 8). Regarding the aro-above-cld-1500 and the aro-above-cld runs, the greater time- and domain-averaged cloud mass is contributed by lower aerosol concentrations and less aerosol radiative heating in the upper atmosphere in the aro-above-cld-1500 run than in the aro-above-cld run (Figure 8). Figure 6 shows that the time- and domain-averaged cloud mass in the aro-above-cld-1500 run is higher than in the control run. This is due to more solar radiation reaching the surface in the aro-above-cld-1500 run (Table 2). The higher average cloud mass in the aro-above-cld-1500 run is despite higher aerosol concentrations and more aerosol radiative heating not only in the low atmosphere in the control run, but also in the upper atmosphere in the aro-above-cld-1500 run (Figure 8). Figure 6 also shows that the time- and domain-averaged cloud mass

Deleted: rioid.

Deleted: The average radiative heating rate is higher in the aro-above-cld run than in the control run at altitudes between ~2.5 and 3.5 km. This is associated with the fact that the main aerosol layer is located at altitudes between 2.5 and 3.5 km in the aro-above-cld run.

Deleted: e

Deleted: more

Deleted: than in the control run

Deleted: lower

Deleted: ¶

Deleted: Effects of greater radiative heating in the low atmosphere on CAPE outweigh those effects of solar radiation which are incident on the surface and the associated surface heat fluxes during the initial stage in the control run. This leads to more intense clouds with more cloud mass for the rest of periods, in turn leading to the more time- and domain-averaged cloud mass in the control run than in the aro-above-cld run.¶

Deleted: e main

Deleted: reaching the surface

Deleted: makes

Deleted: higher

Deleted:

Deleted: between 13:50 and 14:20 LST during which

Deleted: run exists

Deleted: 5d

Deleted: Then, there are stronger updrafts and greater condensation rate and cloud-liquid mass density developing in the control-1500 run than in the control run over most of the simulation period, which are except for the period between 13:50 and 14:20 LST during which the jump in updrafts and cloud-liquid mass in the control run exists, and in the aro-above-cld-1500 run than in the aro-above-cld run throughout the simulation period (Figures 5a, 5b and 5c).

Deleted: -liquid

Deleted: density

Deleted: in the control-1500 run than in the control run and in the

Deleted: 4

Deleted: in the main aerosol layer

Deleted: 6

Deleted: In

Deleted: 4

Deleted: , it is seen

Deleted: -liquid

Deleted: than in the control run and despite the fact that aerosol [6]

Deleted: Table 2 and

Deleted: 6

Deleted: In

Deleted: 4

Deleted: , it is also seen

Deleted: -liquid

751 in the control-1500 run is higher than in the aro-above-cld run. This is associated with the  
 752 fact that more solar radiation reaches the surface in the control-1500 run than in the aro-  
 753 above-cld run (Table 2). The higher average cloud mass in the control-1500 run is also  
 754 associated with higher aerosol concentrations and more aerosol radiative heating not only  
 755 in the low atmosphere in the control-1500 run, but also in the upper atmosphere in the aro-  
 756 above-cld run (Figure 8).

757 Similar to the situation between the control and aro-above-cld runs, there is the less  
 758 surface-reaching solar radiation in the control-1500 run than in the aro-above-cld-1500 run  
 759 (Table 2). In association with this, there is the less surface heat fluxes in the control-1500  
 760 run. However, overall, CAPE is higher and cloud mass is greater in the control-1500 run  
 761 than in the aro-above-cld-1500 run (Figures 6, 7a and 7d). This is because similar to the  
 762 situation between the control and aro-above-cld runs, aerosols heat up the low atmosphere  
 763 more in the control-1500 run and the upper atmosphere more in the aro-above-cld-1500  
 764 run (Figure 8c). The CAPE evolution shows that there is no jump in CAPE and thus  
 765 updrafts in the control-1500 run (Figures 7b and 7d). This mainly contributes to smaller  
 766 differences in CAPE, updrafts, condensation and cloud mass between the control-1500 and  
 767 aro-above-cld-1500 runs than between the control and aro-above-cld runs (Figures 6 and  
 768 7).

769 In the control run, the instability or CAPE accumulates or increases rapidly to reach  
 770 its peak for a period between 13:50 and 14:10 LST, while in the control-1500 run, CAPE  
 771 increases gradually to reach its peak from ~12:00 LST to ~14:30 LST (Figure 7d). For a  
 772 period between ~14:10 and ~14:50 LST, CAPE reduces rapidly down back to the CAPE  
 773 value around ~13:50 LST in the control run. However, CAPE decreases gradually and  
 774 never drops back to the CAPE value at ~12:00 LST until the end of the simulation period  
 775 in the control-1500 run. This leads to the shorter life cycle or lifetime of the system in the  
 776 control run than in the control-1500 run as well as in the aro-above-cld run. Accompanying  
 777 this is the similar life cycle between the control-1500 and aro-above-cld-1500 runs. Here,  
 778 we see that as aerosol concentration increases in the aerosol layer in the low atmosphere,  
 779 the time scale of the accumulation and consumption of the instability or convective energy  
 780 gets shorter, leading to the shorter lifetime of the cloud system.

Deleted: his i

Deleted: s due to

Deleted: (in the upper atmosphere)

Deleted: (aro-above-cld run) than in the aro-above-cld run

Deleted: (control-1500 run).

Deleted: reaching the surface

Deleted: than in the aro-above-cld-1500 run

Deleted: This favors higher CAPE and more invigoration of updrafts and associated convection in the aro-above-cld-1500 run than in the control-1500 run.

Deleted: 5

Deleted: more

Deleted: are in the low atmosphere

Deleted: than in the aro-above-cld-1500 run

Deleted: These more aerosols heat up the low atmosphere more and increase the instability there more (Figure 6c). This induces increases in CAPE, which compensates for decreases in CAPE due to the smaller amount of solar radiation reaching the surface in the control-1500 run, and leads to overall higher CAPE in the control-1500 run than in the aro-above-cld-1500 run. \*

Associated with higher CAPE, there is greater cloud-liquid mass density in the control-1500 run than in the aro-above-cld-1500 run, which is similar to the situation between the control and aro-above-cld runs. However, differences in the mass density between these repeated runs are smaller than those between the control and aro-above-cld runs (Figure 4). As seen in Figure 5a which shows the time series of the domain-averaged cloud-liquid mass density, the control-1500 run does not show a jump in the mass density unlike the situation in the control run. This contributes to smaller differences in cloud-liquid mass density between the control-1500 and aro-above-cld-1500 runs than between the control and aro-above-cld runs.

Deleted: of the control-1500 and aro-above-cld-1500 runs

Deleted: 5

Deleted: ly contributes to smaller

Deleted: s

Deleted: and

Deleted: which in turn contributes to smaller differences in

Deleted: than between the control and aro-above-cld runs

Deleted: In addition, remember that the cloud system in the control run has a shorter life cycle than in the aro-above-cld run. [7]

Deleted: , which forms the jump,

Deleted: 5

Deleted: 0

Deleted: , while

Deleted: not only

Deleted: n

Deleted: but also in the control run than in the control-1500 run

Deleted: main

Deleted: When aerosol concentration in the main aerosol layer [8]

Deleted: Comparisons among the above four standard simulations [9]



### 869 3.3 Comparisons between simulations with predicted and prescribed aerosol 870 concentrations

871

872 Figure 9 shows the vertical distributions of aerosol concentrations, which are averaged over  
873 the horizontal domain and simulation period, for the standard and repeated runs with no  
874 temporal variation of aerosols. Comparisons between the control and control-novary runs  
875 and between the control-1500 and control-1500-novary runs show that due to the upward  
876 transportation of aerosols by updrafts, aerosol concentrations in the aerosol layer in the low  
877 atmosphere reduces and those in the air above the layer increases (Figures 9a and 9c). Note  
878 that the low atmosphere is where cloud-induced updrafts develop and grow, hence, the  
879 upward transportation of aerosols by them is dominant. This leads to the more low-  
880 atmosphere radiative heating of air by aerosols in the control-novary run than in the control  
881 run and in the control-1500-novary run than in the control-1500 run.

882 Comparisons between the aro-above-cld and aro-above-cld-novary runs and between  
883 the aro-above-cld-1500 and aro-above-cld-1500-novary runs show that due to the  
884 transportation of aerosols by downdrafts, aerosol concentrations in the aerosol layer in the  
885 upper atmosphere reduces and those in the air below the layer increases (Figures 9b and  
886 9d). Note that the upper atmosphere is where cloud-induced updrafts decelerate and turn  
887 into downdrafts, and the downward transportation of aerosols by them is dominant.  
888 However, those increases in aerosol concentrations in the air below the aerosol layer  
889 mainly occur between ~1.5 and ~2.5 km, and aerosol concentrations and the associated  
890 instability in the low atmosphere do not change significantly (Figures 9b and 9d). This  
891 leads to similar instability in the low atmosphere and CAPE, which in turn leads to similar  
892 updrafts and cloud mass between the aro-above-cld and aro-above-cld-novary runs and  
893 between the aro-above-cld-1500 and aro-above-cld-1500-novary runs (Figure 10a).

894 Due to more radiative heating of air in the low atmosphere, there are higher CAPE,  
895 stronger updrafts and higher cloud mass in the control-novary run than in the control run  
896 and in the control-1500-novary run than in the control-1500 run (Figure 10a). It is notable  
897 that cloud mass in the control-novary run is so large that its maximum value in the vertical  
898 profile exceeds that even in the control-1500-novary run (Figure 10a). Associated with this,  
899 there are only ~20 % changes in cloud mass between the control-1500 and control-1500-

Deleted: 7

Deleted: (e.g., the control-novary, aro-above-cld-novary, control-1500-novary, and aro-above-cld-1500-novary runs).

Deleted: (between the control-1500 and control-1500-novary runs)

Deleted: in the control (control-1500) run

Deleted: main

Deleted: ayer in the low atmosphere

Deleted: main aerosol

Deleted: This is as compared to the situation in the control-novary (control-1500-novary) run where aerosols are assumed not to be affected by cloud-induced wind (Figures 7a and 7c).

Deleted: Due to the higher concentration of aerosols in the low atmosphere between 0.0 and ~1.0 km, there is

Deleted: in the low atmosphere

Deleted: (between the aro-above-cld-1500 and aro-above-cld-1500-novary runs)

Deleted: in the aro-above-cld (aro-above-cld-1500) run

Deleted: main

Deleted: main aerosol

Deleted: This is as compared to the situation in the aro-above-cld-novary (aro-above-cld-1500-novary) run where aerosols are assumed not to be affected by cloud-induced wind (Figures 7b and 7d).

Deleted: main

Deleted: for the atmosphere

Deleted: between 0.0 and ~1.0 km

Deleted: 7

Deleted: 7

Deleted: Hence, these transported aerosols by downdrafts do not affect instability in the low atmosphere, which tends to have more impacts on CAPE than instability in other parts of the atmosphere, significantly.

Deleted: 8

Deleted: However, d

Deleted: more aerosols and their

Deleted: in the control-novary run than in the control run and in the control-1500-novary run than in the control-1500 run

Deleted: (or greater instability)

Deleted: 8

Deleted: as shown in Figure 8a

Deleted: 8

940 novary runs, while there are as much as ~200 % changes in cloud mass between the control  
 941 and control-novary runs. This indicates that with higher aerosol concentrations in the low  
 942 atmosphere, changes in cloud mass due to the wind-induced variation of those  
 943 concentrations are much larger.

### 945 3.4 Comparisons between simulations with aerosol radiative effects and those with 946 no aerosol radiative effects

947  
 948 Figure 10b shows that with no aerosol radiative effects, differences in cloud mass due to  
 949 the altitude of the aerosol layer are smaller. However, even with no aerosol radiative effects,  
 950 there is higher cloud mass when the aerosol layer is in the low atmosphere than in the upper  
 951 atmosphere as in the standard runs. Also, cloud mass increases when aerosol radiative  
 952 effects are turned off and this increase enhances as aerosol concentrations increase (Figure  
 953 10b). Here, we see that aerosol radiative effects suppress clouds and reduce cloud mass by  
 954 reducing the surface-reaching solar radiation and the surface heat fluxes. The suppression  
 955 of clouds and reduction in cloud mass are greater with higher aerosol concentrations, since  
 956 more aerosols reduce the surface-reaching solar radiation more.

957 Note that aerosol activation mainly occurs around cloud bases in the low atmosphere  
 958 and more aerosols induce more activation for a given thermodynamic condition. Hence,  
 959 there are more aerosol activation (or nucleation of droplets) and higher cloud droplet  
 960 number concentration (CDNC) when the aerosol layer is in the low atmosphere than in the  
 961 upper atmosphere. The averaged CDNC over grid points with non-zero CDNC and the  
 962 whole simulation period is 532, 57, 131 and 53 cm<sup>-3</sup> in the control-norad, aro-above-cld-  
 963 norad, control-1500-norad and the aro-above-cld-1500-norad runs, respectively. Droplets  
 964 act as a source of condensation, since individual droplets provide their surface areas onto  
 965 which water vapor condenses. Hence, higher CDNC induces more condensation and this  
 966 in turn induces stronger updrafts and more cloud mass with the aerosol layer in the low  
 967 atmosphere than in the upper atmosphere. These effects of more aerosols, which induce  
 968 more condensation and stronger updrafts, are generally referred to as aerosol microphysical  
 969 effects (Lee et al., 2016). The differences in CDNC due to the altitude of the aerosol layer  
 970 increase with increasing aerosol concentrations. This leads to greater differences in

~~Deleted:~~ as

~~Deleted:~~ increases

~~Deleted:~~ the sensitivity of responses of

~~Deleted:~~ changes in

~~Deleted:~~ aerosol

~~Deleted:~~ which are induced by cloud-induced wind, in the low atmosphere

~~Deleted:~~ increases substantially

~~Deleted:~~ 8

~~Deleted:~~

~~Deleted:~~ between the control-norad and aro-above-cld-norad runs are much smaller than those differences between the control and aro-above-cld runs with aerosol radiative effects

~~Deleted:~~ as in the control and aro-above-cld runs, there is higher cloud mass in the control-norad run, which has the main aerosol layer in the low atmosphere, than in the aro-above-cld-norad run, which has the main aerosol layer in the upper atmosphere.

~~Deleted:~~ Figure 8b shows that

~~Deleted:~~ in each of the control and aro-above-cld runs

~~Deleted:~~ significantly

~~Deleted:~~ .

~~Deleted:~~ Figure 8b shows that with no aerosol radiative effects, differences in cloud mass between the control-1500-norad and aro-above-cld-1500-norad runs are also smaller than those differences between the control-1500 and aro-above-cld-1500 runs with aerosol radiative effects. However, as in the control-1500 and aro-above-cld-1500 runs, there is higher cloud mass in the control-1500-norad run, which has the main aerosol layer in the low atmosphere, than in the aro-above-cld-norad run, which has the main aerosol layer in the upper atmosphere (Figure 8b). Figure 8b shows that cloud mass in each of the control-1500 and aro-above-cld-1500 runs increases [10]

~~Deleted:~~ . This means that effects of aerosol-induced reduction [11]

~~Deleted:~~ increase

~~Deleted:~~ increasing

~~Deleted:~~ s in the main aerosol layer

~~Deleted:~~ , whether the main layer is in the low atmosphere or [12]

~~Deleted:~~ and surface heat fluxes

**Moved (insertion) [2]**

~~Deleted:~~ which are located

~~Deleted:~~ .

~~Deleted:~~ More aerosols and their

~~Deleted:~~ produce

~~Deleted:~~ in the low atmosphere

~~Deleted:~~ in the control-1500-norad run than in the aro-above-cld-1500-norad run [13]

**Formatted:** Superscript

**Moved up [2]:** Note that aerosol activation mainly occurs around

~~Deleted:~~ in the control-1500-norad run than in the aro-above-cld-1500-norad run [14]

~~Deleted:~~ s

~~Deleted:~~ are greater due to greater differences in aerosols in the [15]

~~Deleted:~~ greater aerosol microphysical effects or



condensation, associated updrafts and cloud mass due to the altitude of the aerosol layer with higher aerosol concentrations when there are no aerosol radiative effects (Figure 10b).

Here, we see that differences in cloud mass due to the altitude of the aerosol layer are greater when aerosol microphysical and radiative effects work together than when aerosol microphysical effects work alone (Figure 10b). Also, remember that the initial concentration of aerosols in the aro-above-cld-norad run is identical to that in the aro-above-cld-1500-norad run in the low atmosphere. Due to this, CDNC, condensation and cloud mass in the aro-above-cld-norad run are similar to those in the aro-above-cld-1500-norad run (Figure 10b).

#### 4. Summary and conclusions

This study examined how impacts of aerosols on warm cumulus clouds in the Korean Peninsula vary with the altitude of an aerosol layer. It is found that the aerosol layer intercepts the surface-reaching solar radiation more when the layer is in the low atmosphere than in the upper atmosphere. With the aerosol layer in the low atmosphere, this makes the surface heat fluxes and associated CAPE lower, which tend to make updrafts weaker and cloud mass lower. However, the layer in the low atmosphere heats up the air there more to produce the higher CAPE and cloud mass.

With decreasing concentrations of aerosols in the aerosol layer, there are decreases in the interception of the surface-reaching solar radiation, increases in surface heat fluxes, CAPE and cloud mass. However, the decreasing concentrations of aerosols cause the jump in CAPE to disappear when the layer is in the low atmosphere. This makes differences in cloud mass due to the altitude of the layer reduce. When the aerosol layer is in the low atmosphere, with increasing aerosol concentrations in the layer, the lifetime of cloud system reduces and becomes shorter than when the layer is in the upper atmosphere.

Updrafts and downdrafts in clouds transport aerosols. In particular, for the aerosol layer in the low atmosphere, updrafts transport aerosols in the layer to places above it. This reduces aerosol concentrations in the layer, leading to reduction in radiative heating of air by aerosols, CAPE, updrafts and cloud mass. This reduction enhances with increasing aerosol concentrations in the layer. For the aerosol layer in the upper atmosphere,

**Deleted:** mass between the control-norad and aro-above-cld-norad runs than those between the control-1500-norad and aro-above-cld-1500-norad runs. With aerosol radiative effects, radiative heating of air in the low atmosphere works in tandem with aerosol microphysical effects. Hence, it is shown that as compared to the situation with no aerosol radiative effects, with aerosol radiative effects,

**Deleted:** d

**Deleted:** between the run with the main aerosol layer in the low atmosphere and that with the layer in the upper atmosphere are greater, whether aerosol concentrations are low (initially set at  $1500 \text{ cm}^{-3}$ ) or high (initial set at  $15000 \text{ cm}^{-3}$ ) in the layer. In addition to the jump in CAPE, updrafts and condensation in the control run as described in Section 3.1, greater aerosol microphysical effects in the low atmosphere when aerosol concentrations are high (initial set at  $15000 \text{ cm}^{-3}$ ) in the aerosol layer contributes to greater differences in cloud mass between the control and aro-above-cld runs than between

**Deleted:** T

**Deleted:** where most of aerosol activation occurs as seen in the [17]

**Deleted:** in the low atmosphere,

**Deleted:** and

**Deleted:** . This leads to similar cloud mass between the runs

**Deleted:** .

**Deleted:** differential impacts of an aerosol layer on warm cumulus

**Deleted:** between a situation where the main aerosol layer is... [19]

**Deleted:** This study finds

**Deleted:** main

**Deleted:** more

**Deleted:** which reaches the surface

**Deleted:** it

**Deleted:** when it is in

**Deleted:** T

**Deleted:** make

**Deleted:** when the main aerosol layer is in the low atmosphere

**Deleted:** with the main aerosol layer in the low atmosphere, the [20]

**Deleted:** main

**Deleted:** reaching the surface

**Deleted:** whether the main layer is in the low atmosphere or in the [21]

**Deleted:** in instability as seen in the evolution of

**Deleted:** main

**Deleted:** leads to reducing

**Deleted:** between the situation with the main layer in the low... [22]

**Deleted:** main

**Deleted:** aerosol

**Deleted:** in a way that the lifetime with the main layer in the low... [23]

**Deleted:** main

**Deleted:** main

**Deleted:** main

**Deleted:** main

1167 downdrafts transport aerosols in the layer to places below it. However, this does not affect  
 1168 aerosol concentrations and radiative heating of air in the low atmosphere significantly. This  
 1169 in turn has negligible effects on CAPE and cloud mass.

1170 Aerosol radiative effects suppress clouds and reduce cloud mass by cutting down the  
 1171 surface-reaching solar radiation. This suppression of clouds increases with increasing  
 1172 aerosol concentrations in the aerosol layer. Aerosol microphysical effects enhance cloud  
 1173 mass and these effects are stronger with higher aerosol concentrations. Differences in cloud  
 1174 mass due to the altitude of the aerosol layer are enhanced when aerosol radiative effects  
 1175 and aerosol microphysical effects work together as compared to when only aerosol  
 1176 microphysical effects are present.

1177 This study shows that aerosol-induced changes in the surface fluxes and those in  
 1178 radiative heating of air interact with each other in terms of responses of convection and  
 1179 clouds to aerosols. This interaction varies with the altitude of aerosols and cloud-induced  
 1180 wind. In general, traditional parameterizations for warm cumulus clouds in climate and  
 1181 weather-forecast models have not been able to consider this dependence of the interaction  
 1182 on the altitude of aerosols, since those parameterizations do not differentiate aerosol layers  
 1183 based on their vertical locations. In addition, the cloud-induced wind at cloud scales has  
 1184 not been represented by those parameterizations with good confidence. So, impacts of  
 1185 aerosol transportation by cloud-induced wind on the interaction have not been properly  
 1186 considered in those traditional parameterizations. This suggests that the vertical locations  
 1187 of aerosols and cloud-induced wind should be added to factors that need to be considered  
 1188 or improved to better parameterize warm cumulus clouds and their interactions with  
 1189 aerosols.

1190

1191

1192

1193

1194

1195

1196

1197

**Deleted:** ,

**Deleted:** does

**Deleted:** not affect

**Deleted:** significantly

**Deleted:** reducing

**Deleted:** which reaches the surface as compared to a situation when there are no aerosol radiative effects

**Deleted:** main

**Deleted:** in the main layer

**Deleted:** W

**Deleted:** , which are in terms of radiative heating of air by aerosols,

**Deleted:** , differences in cloud mass between a situation where the main layer is in the upper atmosphere and that where the main layer is in the low atmosphere enhance as compared to a situation where only aerosol microphysical effects are present. More aerosols, and thus stronger radiative heating of air and stronger aerosol microphysical effects in the main aerosol layer in the low atmosphere enable this enhancement to be larger when aerosol concentrations are high in the main layer than they are low. ¶

**Deleted:** This study shows that radiative heating of air by aerosols in the low atmosphere, which are around or below cloud bases, enhances instability, invigorates convection and increases cloud mass, which is contrary to the conventional wisdom of impacts of absorbing aerosols on convection. However, radiative heating of air by aerosols in the upper atmosphere, which are around or above cloud tops, enhances stability, suppresses convection and reduces cloud mass. Aerosols in the low atmosphere intercept more solar radiation reaching the surface, which tend to suppress the surface fluxes and convection, than aerosols in the upper atmosphere. Here

**Deleted:** , we see that

**Deleted:** varying vertical location

**Deleted:** d the varying

**Deleted:** that is at cloud scale

**Deleted:** vertical

**Deleted:** location

**Deleted:** in general,

**Deleted:** s for warm clouds

**Deleted:** cloud-scale

**Deleted:** , which is not able to be resolved by general resolutions in climate and weather-forecast models,

**Deleted:** ve

**Deleted:**

**Deleted:** Results here demonstrate that for more comprehensive representation of interactions between warm cumulus clouds and aerosols, we need to develop a more comprehensive parameterization that is able well represent the varying interaction between aerosol-induced changes in the surface fluxes and those in radiative heating of air with varying vertical locations of aerosols and aerosol transportation by cloud-induced wind. ¶

1248 **Code/Data source and availability**

1249

1250 Our private computer system stores the code/data which are private and used in this study.

1251 Upon approval from funding sources, the data will be opened to the public. Projects related

1252 to this paper have not been finished, thus, the sources prevent the data from being open to

1253 the public currently. However, if information on the data is needed, contact the

1254 corresponding author Seoung Soo Lee (slee1247@umd.edu).

1255

1256 **Author contributions**

1257 Essential initiative ideas are provided by SSL, JU and WJC to start this work. Simulation

1258 and observation data are analyzed by SSL, JU and KJH. CHJ. JG and YZ review the results

1259 and contribute to their improvement.

1260

1261 **Competing interests**

1262 The authors declare that they have no conflict of interest.

1263

1264

1265

1266

1267

1268

1269

1270

1271

1272

1273

1274

1275

1276

1277

1278

1279

1280

1281

1282

1283

1284

1285

1286

1287

Deleted: ¶



1291 **Acknowledgements**

1292

1293 This study is supported by the National Research Foundation of Korea (NRF) grant funded  
1294 by the Korea government (MSIT) (No. NRF2020R1A2C1003215 and No.  
1295 2020R1A2C1013278) and the Korea Institute of Marine Science and Technology  
1296 Promotion(KIMST) funded by the Ministry of Oceans and Fisheries (20210607). This  
1297 study is also supported by Basic Science Research Program through the NRF funded by  
1298 the Ministry of Education (No. 2020R1A6A1A03044834).

1299

1300

1301

1302

1303

1304

1305

1306

1307

1308

1309

1310

1311

1312

1313

1314

1315

1316

1317

1318

1319

1320

1321

**Formatted:** Body Text 3, Left, Level 2

**Formatted:** Font: (Default) Times New Roman, (Asian) Times New Roman, 12 pt, Font color: Auto, Pattern: Clear

**Formatted:** Font: (Default) Times New Roman, (Asian) Times New Roman, 12 pt, Font color: Auto, Pattern: Clear

**Formatted:** Font: (Default) Times New Roman, (Asian) Times New Roman, 12 pt, Font color: Auto, Pattern: Clear

**Formatted:** Font: (Default) Times New Roman, (Asian) Times New Roman, 12 pt, Font color: Auto, Pattern: Clear

**Deleted:** the "Construction of Ocean Research Stations and their Application Studies" project, funded by the Ministry of Oceans and Fisheries, South Korea.

1325 **References**

1326

1327 Albrecht, B. A.: Aerosols, cloud microphysics, and fractional cloudiness, *Science*, 245,  
1328 1227-1230, 1989.

1329 Brown, A., Milton, S., Cullen, M., Golding, B., Mitchell, J., and Shelly, A.: Unified  
1330 modeling and prediction of weather and climate: A 25-year journey, *Bull. Am*  
1331 *Meteorol. Soc.* 93, 1865–1877, 2012.

1332 [Chaboureau, J.-P., Labbouz, L., Flamant, C., and Hodzic, A.: Acceleration of the southern](#)  
1333 [African easterly jet driven by the radiative effect of biomass burning aerosols and its](#)  
1334 [impact on transport during AEROCLO-sA, \*Atmos. Chem. Phys.\*, 22, 8639–8658,](#)  
1335 <https://doi.org/10.5194/acp-22-8639-2022>, 2022.

1336 [Che, H., Stier, P., Watson-Parris, D., Gordon, H., and Deaconu, L.: Source attribution of](#)  
1337 [cloud condensation nuclei and their impact on stratocumulus clouds and radiation in](#)  
1338 [the south-eastern Atlantic, \*Atmos. Chem. Phys.\*, 22, 10789–10807,](#)  
1339 <https://doi.org/10.5194/acp-22-10789-2022>, 2022.

1340 Chen, F., and Dudhia, J.: Coupling an advanced land-surface hydrology model with the  
1341 Penn State-NCAR MM5 modeling system. Part I: Model description and  
1342 implementation, *Mon. Wea. Rev.*, 129, 569–585, 2001.

1343 de Graaf, M., Bellouin, N., Tilstra, L.G., Haywood, J., Stammes, P.: Aerosol direct radiative  
1344 effect of smoke over clouds over the southeast Atlantic Ocean from 2006 to 2009.  
1345 *Geophys. Res. Lett.* 41, 7723-7730, 2014.

1346 [Deaconu, L. T., Ferlay, N., Waquet, F., Peers, F., Thieuleux, F., and Goloub, P.: Satellite](#)  
1347 [inference of water vapour and above cloud aerosol combined effect on radiative](#)  
1348 [budget and cloud top processes in the southeastern Atlantic Ocean, \*Atmos. Chem.\*](#)  
1349 [Phys., 19, 11613–11634, <https://doi.org/10.5194/acp-19-11613-2019>, 2019.](#)

1350 [Denjean, C., Bourrienne, T., Burnet, F., Mallet, M., Maury, N., Colomb, A., Dominutti, P.,](#)  
1351 [Brito, J., Dupuy, R., Sellegri, K., Schwarzenboeck, A., Flamant, C., and Knippertz, P.:](#)  
1352 [Overview of aerosol optical properties over southern West Africa from DACCWA](#)  
1353 [aircraft measurements, \*Atmos. Chem. Phys.\*, 20, 4735–4756,](#)  
1354 <https://doi.org/10.5194/acp-20-4735-2020>, 2020.

1355 [Feingold, G., H. Jiang, H., and J. Y. Harrington, J. Y.: On smoke suppression of clouds in](#)

**Formatted:** Font: (Default) Times New Roman, (Asian) Malgun Gothic, 12 pt, Font color: Black, Pattern: Clear

**Formatted:** Justified, Indent: Left: 0", Hanging: 2 ch, First line: -2 ch, Line spacing: 1.5 lines, No widow/orphan control, Don't adjust space between Latin and Asian text, Don't adjust space between Asian text and numbers

**Formatted:** Font: (Asian) Malgun Gothic, Font color: Black

**Deleted:** Fan, J., Yuan, T., Comstock, J. M., et al.: Dominant role by vertical wind shear in regulating aerosol effects on deep convective clouds, *J. Geophys. Res.*, 114, doi:10.1029/2009JD012352, 2009.

- 1360 Amazonia, *Geophys. Res. Lett.*, 32, L02804, doi:10.1029/2004GL021369, 2005.
- 1361 Forster, P., et al., Changes in atmospheric constituents and in radiative forcing, in: *Climate*  
 1362 *change 2007: the physical science basis*, Contribution of working group I to the Fourth  
 1363 Assessment Report of the Intergovernmental Panel on Climate Change, edited by  
 1364 Solomon, S., et al., Cambridge Univ. Press, New York, 2007.
- 1365 Formenti, P., B. D'Anna, C. Flamant, et al.: The Aerosols, Radiation and Clouds in  
 1366 Southern Africa Field Campaign in Namibia: Overview, illustrative observations, and  
 1367 way forward, *Bull. Amer. Meteor. Soc.*, 100, 1277-1298, 2019.
- 1368 Hahn, C. J., and Warren, S. G.: A gridded climatology of clouds over land (1971–96) and  
 1369 ocean (1954–97) from surface observations worldwide. *Numeric Data Package NDP-*  
 1370 *026EORNL/CDIAC-153*, CDIAC, Department of Energy, Oak Ridge, TN, 2007.
- 1371 Hansen, J. E., Sato, M. and Ruedy, R.: Radiative forcing and climate response, *J. Geophys.*  
 1372 *Res.*, 102, 6831–6864, 1997.
- 1373 Hartmann, D. L., Ockert-Bell, M. E., and Michelsen, M. L.: The effect of cloud type on  
 1374 earth's energy balance—Global analysis, *J. Climate*, 5, 1281–1304, 1992.
- 1375 Haslett, S. L., Taylor, J. W., Evans, M., Morris, E., Vogel, B., Dajuma, A., Brito, J.,  
 1376 Batenburg, A. M., Borrmann, S., Schneider, J., Schulz, C., Denjean, C., Bourriane,  
 1377 T., Knippertz, P., Dupuy, R., Schwarzenböck, A., Sauer, D., Flamant, C., Dorsey, J.,  
 1378 Crawford, I., and Coe, H.: Remote biomass burning dominates southern West African  
 1379 air pollution during the monsoon, *Atmos. Chem. Phys.*, 19, 15217–15234,  
 1380 <https://doi.org/10.5194/acp-19-15217-2019>, 2019.
- 1381 Haywood, J. M. and Shine, K. P.: Multi-spectral calculations of the radiative forcing of  
 1382 tropospheric sulfate and soot aerosols using a column model, *Q. J. R. Meteorol. Soc.*,  
 1383 123, 1907–1930, 1997.
- 1384 Holben, B. N., Tanré, D., Smirnov, et al.: An emerging ground-based aerosol climatology:  
 1385 Aerosol optical depth from AERONET, *J. Geophys. Res.*, 106, 12067–12097, 2001.
- 1386 Johnson, B. T., Shine, K. P., and Forster, P. M.: The semi-direct aerosol effect: Impact of  
 1387 absorbing aerosols on marine stratocumulus, *Q. J. R. Meteorol. Soc.*, 130, 1407– 1422,  
 1388 2004.
- 1389 Khain, A., Pokrovsky, A., Rosenfeld, D., Blahak, U., and Ryzhko, A.: The role of CCN in  
 1390 precipitation and hail in a mid-latitude storm as seen in simulations using a spectral

**Formatted:** Font: (Asian) Malgun Gothic, 12 pt, Not Italic, Font color: Black

**Formatted:** Font: (Asian) Malgun Gothic, 12 pt, Not Italic, Font color: Black

**Formatted:** Indent: Left: 0", Hanging: 2 ch

**Formatted:** Font: (Asian) Malgun Gothic, 12 pt, Not Italic, Font color: Black

**Formatted:** Font: (Asian) Malgun Gothic, 12 pt, Not Italic, Font color: Black

**Formatted:** Font: (Asian) Malgun Gothic, 12 pt, Not Italic, Font color: Black

**Formatted:** Font: (Asian) Malgun Gothic, 12 pt, Not Italic, Font color: Black

**Formatted:** Font: (Asian) Malgun Gothic, 12 pt, Not Italic, Font color: Black

- 1391 (bin) microphysics model in a 2D dynamic frame, *Atmos. Res.*, 99, 129–146, 2011.
- 1392 Lee, S. S., Guo, J. M., and Li, Z.: Delaying precipitation by air pollution over the Pearl  
1393 River Delta. Part II: Model simulations, *J. Geophys. Res.*, 121, 11739–11760.
- 1394 Lee, S. S., Ha, K.-J., Manoj, M. G., et al.: Midlatitude mixed-phase stratocumulus  
1395 clouds and their interactions with aerosols: how ice processes affect microphysical,  
1396 dynamic, and thermodynamic development in those clouds and interactions?, *Atmos.*  
1397 *Phys. Chem.*, 21, 16843–16868, 2021.
- 1398 Mari, C. H., Cailley, G., Corre, L., Saunio, M., Attié, J. L., Thouret, V., and Stohl, A.:  
1399 Tracing biomass burning plumes from the Southern Hemisphere during the AMMA  
1400 2006 wet season experiment, *Atmos. Chem. Phys.*, 8, 3951–3961,  
1401 <https://doi.org/10.5194/acp-8-3951-2008>, 2008.
- 1402 McFarquhar, G. M. and Wang, H.: Effects of Aerosols on Trade Wind Cumuli over the  
1403 Indian Ocean: Model Simulations, *Q. J. R. Meteorol. Soc.*, 132, 821–843, 2006.
- 1404 Menut, L., Flamant, C., Turquety, S., Deroubaix, A., Chazette, P., and Meynadier, R.:  
1405 Impact of biomass burning on pollutant surface concentrations in megacities of the  
1406 Gulf of Guinea, *Atmos. Chem. Phys.*, 18, 2687–2707, [https://doi.org/10.5194/acp-18-](https://doi.org/10.5194/acp-18-2687-2018)  
1407 [2687-2018](https://doi.org/10.5194/acp-18-2687-2018), 2018.
- 1408 Mlawer, E. J., Taubman, S. J., Brown, P. D., Iacono, M. J., and Clough, S. A.: RRTM, a  
1409 validated correlated-k model for the longwave, *J. Geophys. Res.*, 102, 16663–1668,  
1410 1997.
- 1411 Ramaswamy, V., et al.: Radiative forcing of climate change, in *Climate Change 2001: The*  
1412 *Scientific Basis*, edited by J. T. Houghton et al., 349–416, Cambridge Univ. Press,  
1413 New York, 2001.
- 1414 Redemann, J., Wood, R., Zuidema, P., et al.: An overview of the ORACLES (ObseRvations  
1415 of Aerosols above CLouds and their intEractionS) project: aerosol–cloud–radiation  
1416 interactions in the southeast Atlantic basin, *Atmos. Chem. Phys.*, 21, 1507–1563, 2021.
- 1417 Roberts, G. C. and Nenes, A.: A Continuous-Flow Streamwise Thermal-Gradient CCN  
1418 Chamber for Atmospheric Measurements, *Aerosol Sci. Technol.*, 39, 206–221  
1419 <https://doi.org/10.1080/027868290913988>, 2005.
- 1420 Stephens, G. L., and Greenwald, T. J.: Observations of the Earth’s radiation budget in  
1421 relation to atmospheric hydrology. Part II: Cloud effects and cloud feedback. *J.*

**Formatted:** Font: (Asian) Malgun Gothic, 12 pt, Font color: Black, (Asian) Korean

**Formatted:** Indent: Left: 0", Hanging: 2 ch

**Formatted:** Font: (Asian) Malgun Gothic, 12 pt, Font color: Black, (Asian) Korean

**Formatted:** Indent: Left: 0", Hanging: 2 ch

**Formatted:** Font: (Asian) Malgun Gothic, 12 pt, Font color: Black, (Asian) Korean

**Formatted:** Font: (Asian) Malgun Gothic, 12 pt, Font color: Black, (Asian) Korean

**Formatted:** Font: (Asian) Malgun Gothic, 12 pt, Font color: Black, (Asian) Korean

**Formatted:** Font: (Asian) Malgun Gothic, 12 pt, Not Italic, Font color: Black

**Formatted:** Indent: Left: 0", Hanging: 2 ch

**Formatted:** Font: (Asian) Malgun Gothic, 12 pt, Not Italic, Font color: Black

**Formatted:** Font: (Asian) Malgun Gothic, 12 pt, Not Italic, Font color: Black

**Formatted:** Font: (Asian) Malgun Gothic, 12 pt, Not Italic, Font color: Black

- 1422 Geophys. Res., 96, 15 325–15 340, 1991.
- 1423 Tao, W.-K., Chen, J.-P., Li, Z., Wang, C., and Zhang C., Impact of aerosols on convective  
1424 clouds and precipitation, Rev. Geophys., 50, RG2001, doi:10.1029/2011RG000369,  
1425 2012.
- 1426 Twomey, S.: The influence of pollution on the shortwave albedo of clouds, J. Atmos. Sci.,  
1427 34, 1149-1152, 1977.
- 1428 Twomey, S.: Pollution and the Planetary Albedo, Atmos. Env., 8, 1251-1256, 1974.
- 1429 [van der Werf, G. R., Randerson, J. T., Giglio, L., Collatz, G. J., Mu, M., Kasibhatla, P. S.,  
1430 Morton, D. C., DeFries, R. S., Jin, Y., and van Leeuwen, T. T.: Global fire emissions  
1431 and the contribution of deforestation, savanna, forest, agricultural, and peat fires  
1432 \(1997–2009\), Atmos. Chem. Phys., 10, 11707–11735, \[https://doi.org/10.5194/acp-10-  
1433 11707-2010\]\(https://doi.org/10.5194/acp-10-11707-2010\), 2010.](#)
- 1434 Wang, H., Skamarock, W. C., and Feingold, G.: Evaluation of scalar advection schemes in  
1435 the Advanced Research WRF model using large-eddy simulations of aerosol-cloud  
1436 interactions, Mon. Wea. Rev., 137, 2547-2558, 2009.
- 1437 Warren, S. G., Hahn, C. J., London, J., Chervin, R. M., and Jenne, R. L.: Global distribution  
1438 of total cloud cover and cloud types over land. NCAR Tech. Note NCAR/TN-  
1439 273+STR, National Center for Atmospheric Research, Boulder, CO, 29 pp. + 200  
1440 maps, 1986.
- 1441 [Wilcox, E. M.: Stratocumulus cloud thickening beneath layers of absorbing smoke aerosol,  
1442 Atmos. Chem. Phys., 10, 11769–11777, <https://doi.org/10.5194/acp-10-11769-2010>,  
1443 2010.](#)
- 1444 Wood, R.: Stratocumulus clouds, Mon. Wea. Rev., 140, 2373-2423, 2012.
- 1445 Xu, H., Guo, J., Wang, Y., et al.: Warming effect of dust aerosols modulated by overlapping  
1446 clouds below, Atmos. Env., 166, 2017, 393-402, 2017.
- 1447
- 1448
- 1449
- 1450
- 1451
- 1452
- 1453
- 1454

Deleted: ¶



## FIGURE CAPTIONS

Figure 1. (a) An inner rectangle in the map of the Korean Peninsula represents the simulation domain. The green represents the land area and the light blue the ocean area in the map. A black dot marks the location of a site where the radiosonde sounding is obtained and a red dot the location of the  $PM_{2.5}$  station in the Yellow sea. (b) The simulation domain is shown. The black dots mark the locations of the  $PM_{2.5}$  stations and the red dot the location of the AERONET site in the domain.

Figure 2. Spatial distribution of cloud reflectivity which is unitless and observed by the COMS at 14:00 LST April 13<sup>th</sup>, 2016 in the simulation domain. Contours are at 0.11, 0.15, 0.19 and 0.25.

Figure 3. Vertical distributions of potential temperature and water-vapor mixing ratio at 09:00 LST on April 13<sup>th</sup>, 2016. These distributions are obtained from radiosonde sounding near the simulation domain in Figure 1a.

Figure 4. Time series of  $PM_{2.5}$  observed at the station in the Yellow sea (blue line) and of the average  $PM_{2.5}$  over stations in the simulation domain (red line) between 03:00 LST and 18:00 LST on April 13<sup>th</sup> in 2016.

Figure 5. Aerosol size distribution at the surface. N represents aerosol number concentration per unit volume of air and D represents aerosol diameter.

Figure 6. Vertical distributions of the time- and area-averaged cloud-liquid mass density that represents cloud mass for the standard simulations (i.e., the control, aro-above-cld, control-1500 and aro-above-cld-1500 runs).

Figure 7. Time series of the domain-averaged (a) liquid-water path, (b) updraft speed, (c) condensation rate and (d) CAPE in the standard simulations.

Deleted: ¶

Deleted: (light blue)

Deleted: (ocean)

Formatted: Subscript

Formatted: Font: (Default) Batang, (Asian) Batang

Deleted: ¶

Figure 2. Vertical distributions of potential temperature and water-vapor mixing ratio at 09:00 LST on April 15<sup>th</sup>, 2015. These distributions are obtained from radiosonde sounding near the simulation domain in Figure 1. ¶

Figure 3. Vertical distributions of the area-averaged aerosol concentrations at the first time step of (a) the control run and (b) the aro-above-cld run. ¶

Deleted: 4

Deleted: 5

Deleted: convective available potential energy

1519 Figure 8. Vertical distributions of the time- and area-averaged radiative heating rate (a) in  
 1520 the control and aro-above-cld runs over the initial period between 10:00 and 13:50 LST,  
 1521 (b) in the control and aro-above-cld runs and (c) in the control-1500 and aro-above-cld-  
 1522 1500 runs over the whole simulation period.

Deleted: 6

Deleted: stage

Deleted: over the whole simulation period

1524 Figure 9. Vertical distributions of the time- and area-averaged aerosol concentrations (a)  
 1525 in the control and control-novary runs, (b) aro-above-cld and aro-above-cld-novary runs,  
 1526 (c) control-1500 and control-novary-1500 runs and (d) aro-above-cld-1500 and aro-above-  
 1527 cld-novary-1500 runs.

Deleted: 7

1529 Figure 10. Vertical distributions of the time- and area-averaged cloud-liquid mass density.  
 1530 In (a), the control-novary, aro-above-cld-novary, control-1500-novary and aro-above-cld-  
 1531 1500-novary runs and in (b), the control-norad, aro-above-cld-norad, control-1500-norad  
 1532 and aro-above-cld-1500-norad runs are shown together with the standard simulations.

Deleted: 8

1533

1534

1535

1536

1537

1538

1539

1540

1541

1542

1543

1544

1545

1546

1547

1548

1549

Deleted: 1

Simulations	Altitudes of a aerosol layer (km)	Aerosol concentrations in the aerosol layer at the first time step ( $\text{cm}^{-3}$ )	Aerosol evolution	Aerosol radiative effects
Control	0 - 1	15000	Present	Present
Aro-above-cld	2.5-3.5	15000	Present	Present
Control-1500	0 - 1	1500	Present	Present
Aro-above-cld-1500	2.5-3.5	1500	Present	Present
Control-novary	0 - 1	15000	Absent	Present
Aro-above-cld-novary	2.5-3.5	15000	Absent	Present
Control-1500-novary	0 - 1	1500	Absent	Present
Aro-above-cld-1500-novary	2.5-3.5	1500	Absent	Present
Control-norad	0 - 1	15000	Present	Absent
Aro-above-cld-norad	2.5-3.5	15000	Present	Absent
Control-1500-norad	0 - 1	1500	Present	Absent
Aro-above-cld-1500-norad	2.5-3.5	1500	Present	Absent

Deleted: main

Deleted: main

1567

1568 Table 1. Summary of simulations

1569

1570

1571

1572

1573

1574

1575

1576

1577

1578

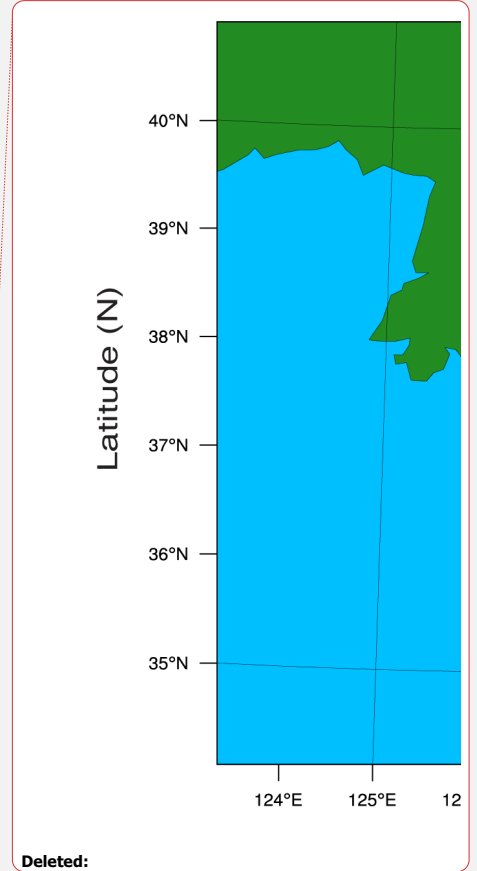
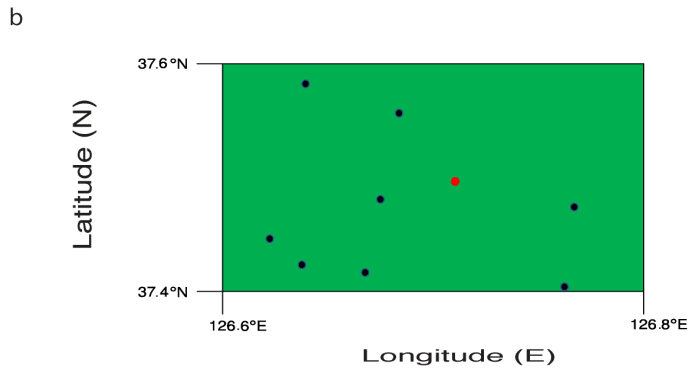
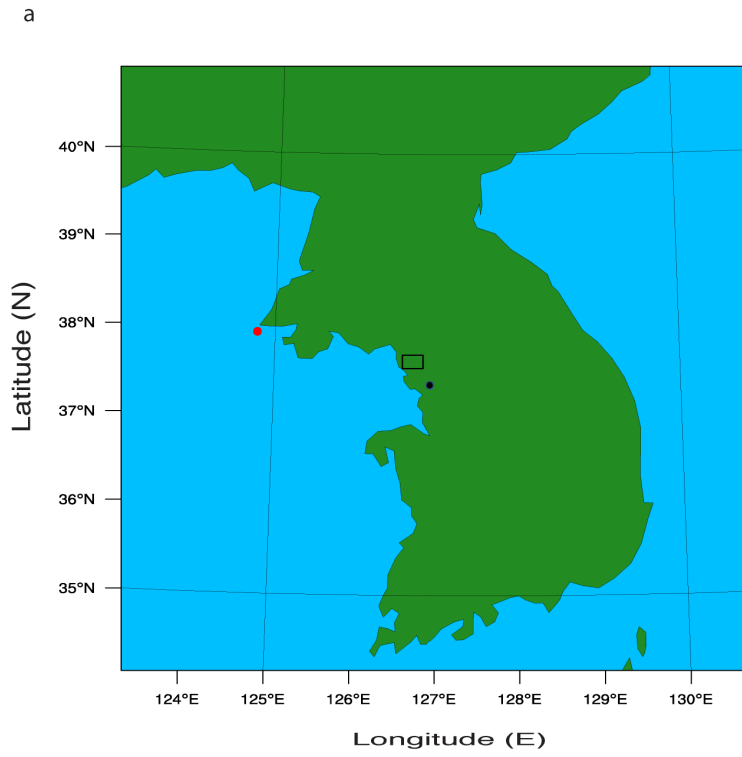
1579

1580

Simulations	Net solar radiation flux reaching the surface (W m <sup>-2</sup> )	Surface latent heat fluxes (W m <sup>-2</sup> )	Surface sensible heat fluxes (W m <sup>-2</sup> )	Surface latent heat fluxes plus surface sensible heat fluxes (W m <sup>-2</sup> )
Control	293 (205)	175 (120)	22 (16)	197 (136)
Aro-above-cld	306 (217)	170 (117)	48 (33)	218 (150)
Control-1500	461	250	70	320
Aro-above-cld-1500	467	248	75	323

1583

1584 Table 2. The time- and area-averaged net solar radiation, latent heat, sensible heat and total  
1585 heat (sensible plus latent heat) fluxes at the surface over the whole simulation period in the  
1586 standard simulations. Numbers in the parentheses are averaged over the initial period  
1587 between 10:00 and 13:50 LST for [the](#) control and aro-above-cld runs.



Deleted:

Deleted:

Deleted:

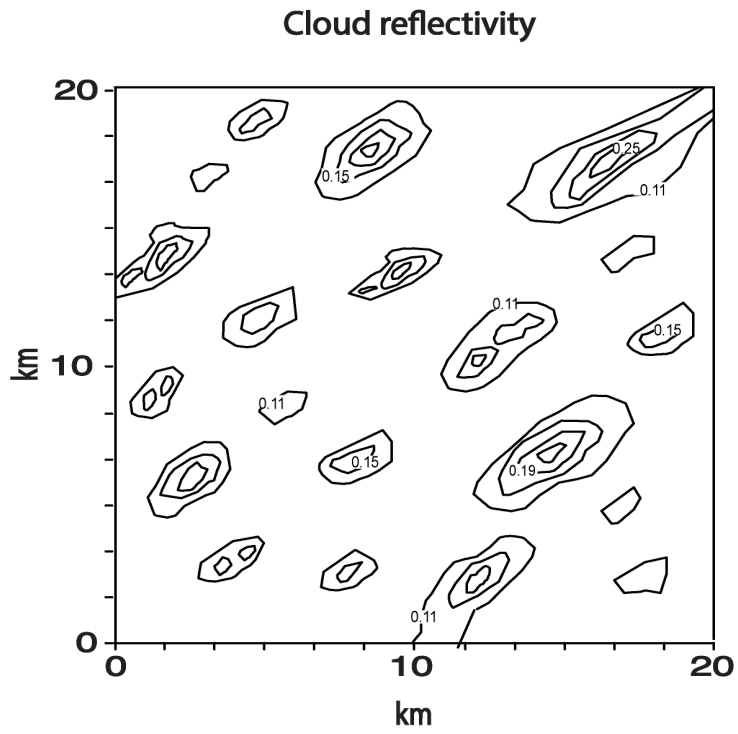
Deleted:

Figure 1

1588

1589

1590



1595

1596

1597

**Figure 2**

Deleted: ¶



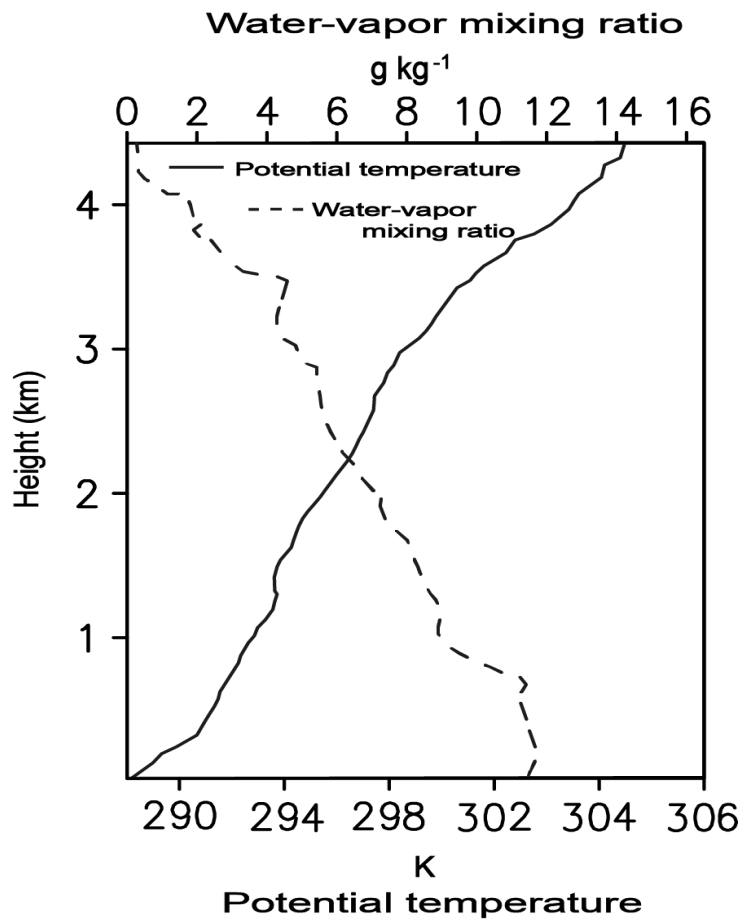


Figure 3

Deleted: 2

1601

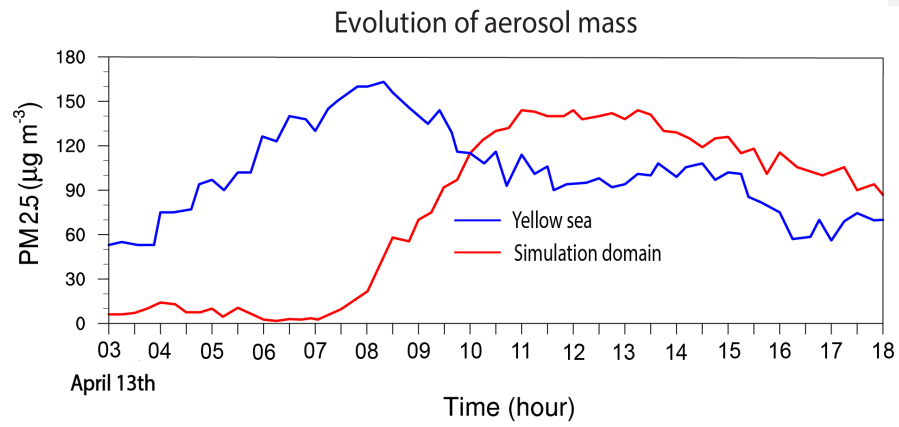
1602

1603

1604

1605

1606



1608

1609

**Figure 4**

1610

1611

1612

1613

1614

1615

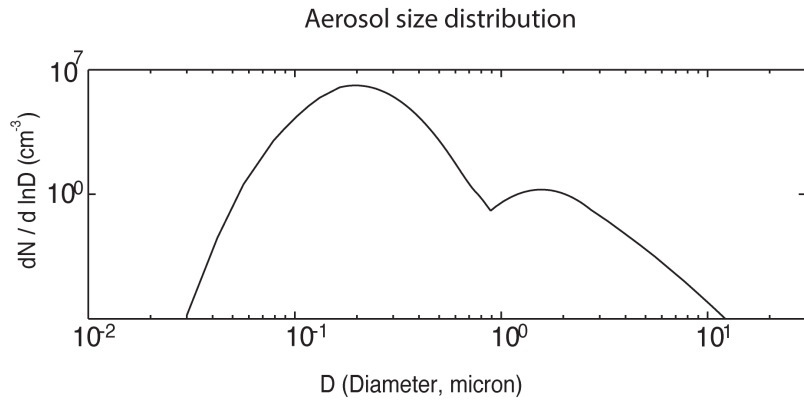
1616

1617

1618

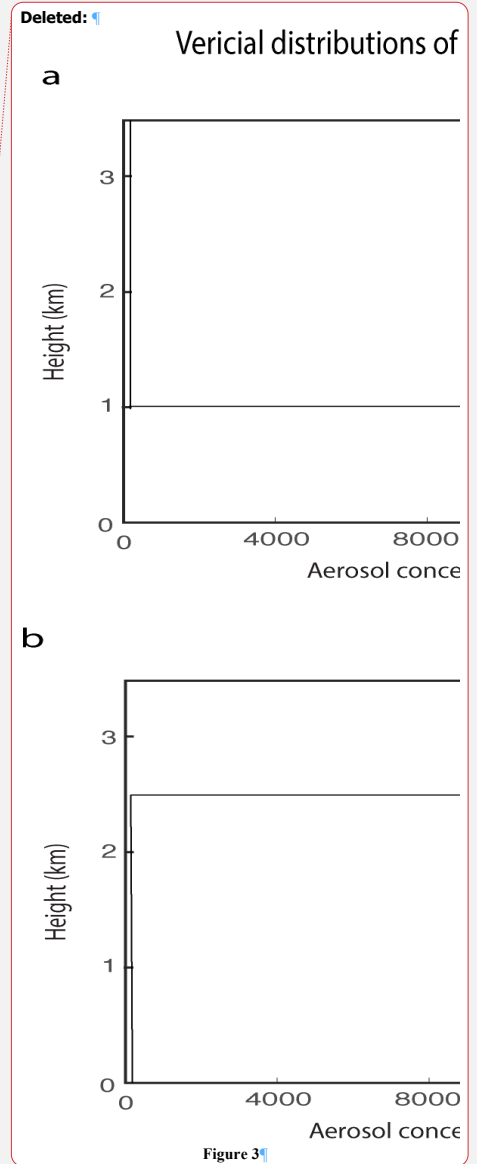
1619

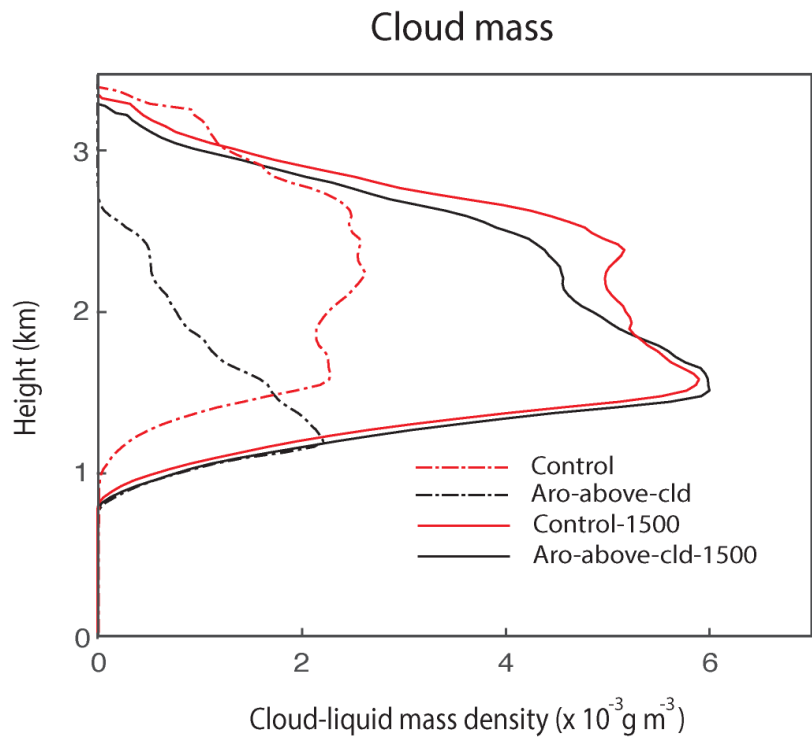




**Figure 5**

1620  
1621  
1622  
1623  
1624  
1625

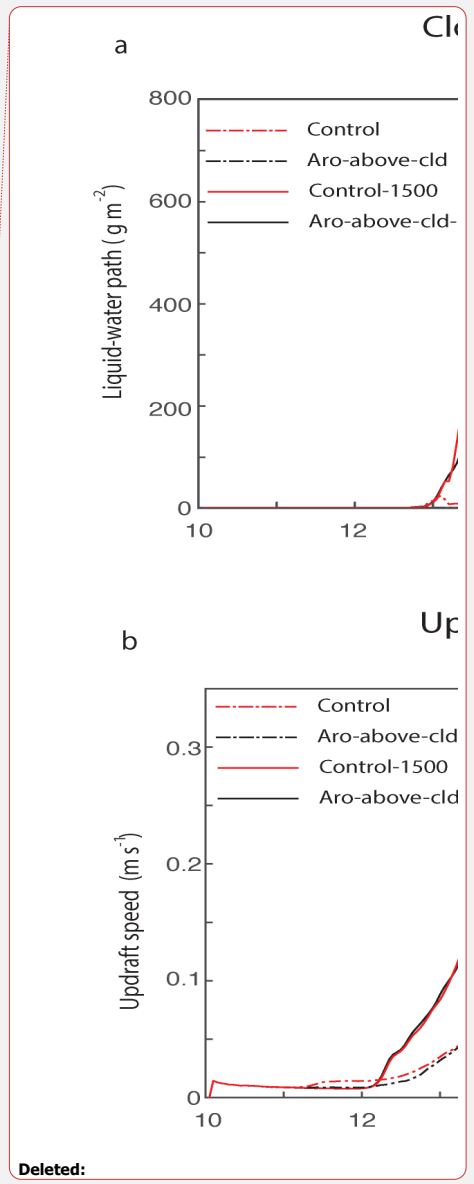
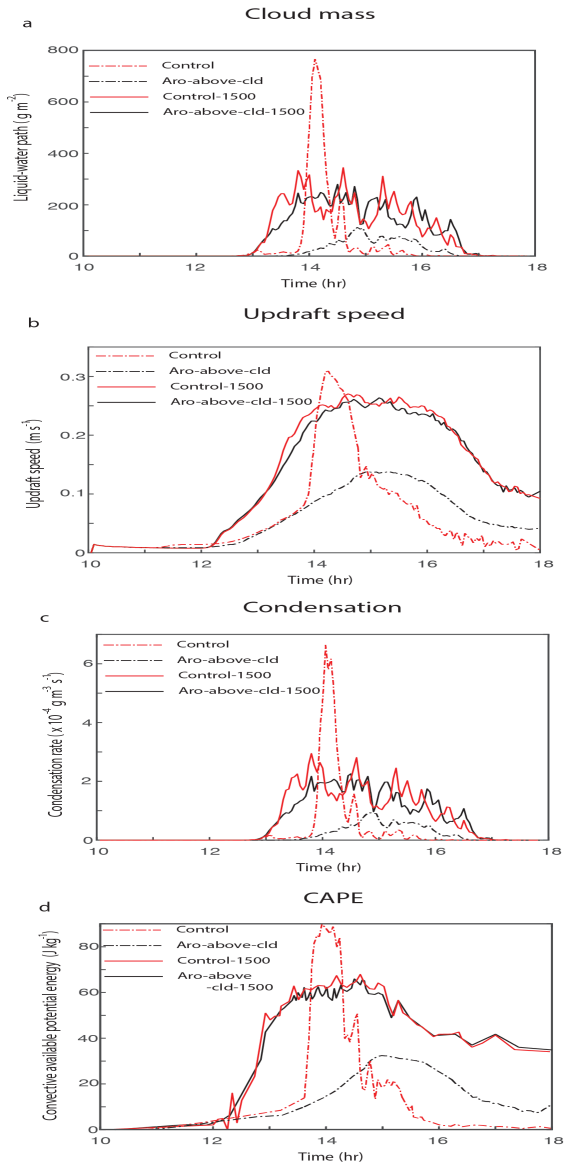




1629  
1630  
1631  
1632  
1633  
1634  
1635  
1636

**Figure 6**

Deleted: 4



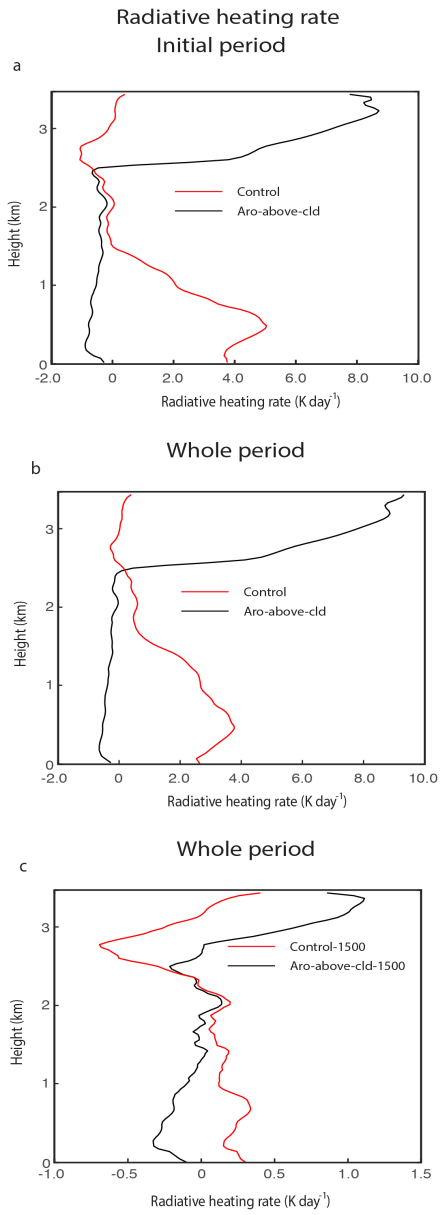
Deleted:

Deleted:  
 Deleted: 5%  
 ... [24]

**Figure 7**

1638

1639



1648  
1649  
1650

**Figure 8**

Deleted: 6

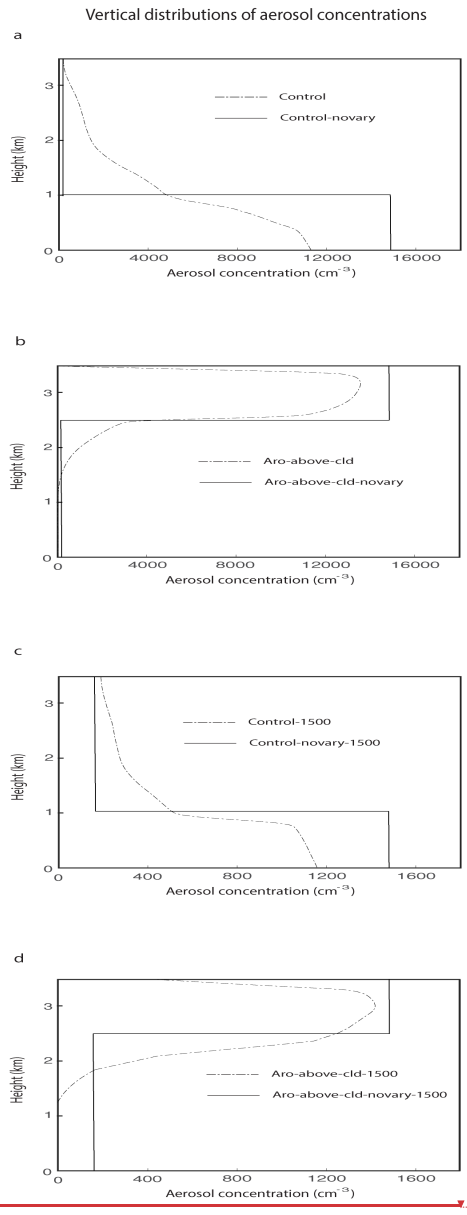
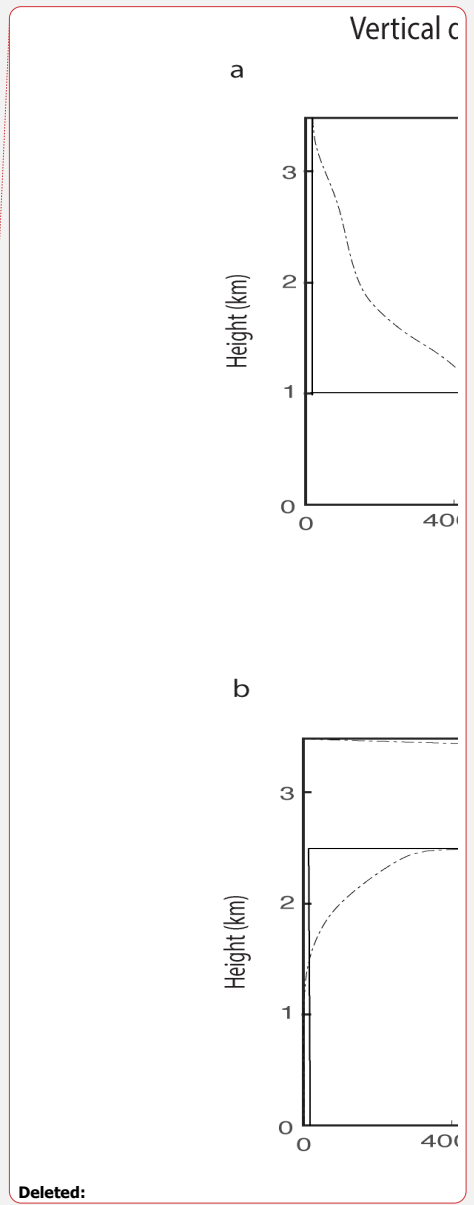


Figure 2



Deleted:

Deleted:

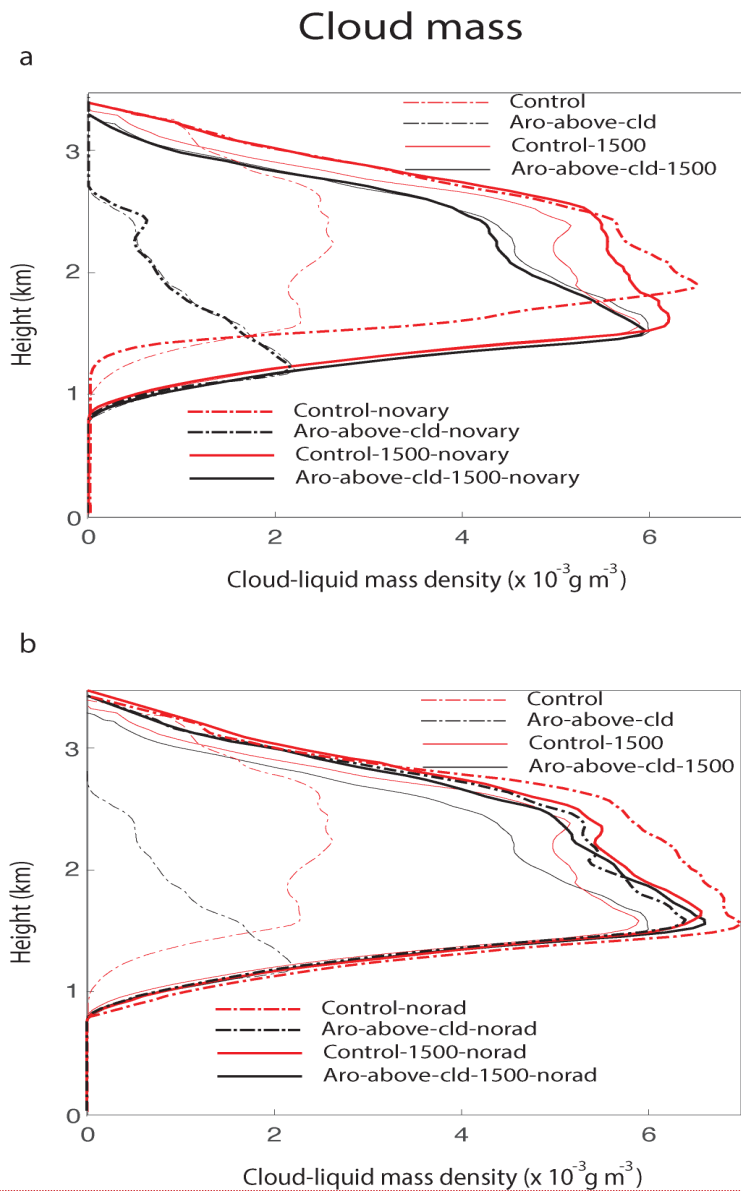
Deleted: 71

... [25]

1652

1653

1654



Deleted: Figure 7

Deleted: 8

1660  
1661  
1662

**Figure 10**



▲ Page 17: [17] Deleted Seoung Soo Lee 8/8/22 9:47:00 AM

▼  
▲ Page 17: [18] Deleted Seoung Soo Lee 8/8/22 4:30:00 PM

▼  
▲ Page 17: [19] Deleted Seoung Soo Lee 8/8/22 4:32:00 PM

▼  
▲ Page 17: [20] Deleted Seoung Soo Lee 8/30/22 9:41:00 AM

▼  
▲ Page 17: [21] Deleted Seoung Soo Lee 8/9/22 7:58:00 AM

▼  
▲ Page 17: [22] Deleted Seoung Soo Lee 8/9/22 8:01:00 AM

▼  
▲ Page 17: [23] Deleted Seoung Soo Lee 8/9/22 8:09:00 AM

▼  
▲ Page 35: [24] Deleted Seoung Soo Lee 7/31/22 7:19:00 AM

▼  
▲ Page 37: [25] Deleted Seoung Soo Lee 7/31/22 7:20:00 AM